ARTICLE

Postsynaptic synaptotagmins mediate AMPA receptor exocytosis during LTP

Dick Wu[1,2,3]*, Taulant Bacaj[1]*, Wade Morishita[2,3]*, Debanjan Goswami[2,3], Kristin L. Arendt[4], Wei Xu[1]†, Lu Chen[4], Robert C. Malenka[2,3] & Thomas C. Südhof[1]

Strengthening of synaptic connections by NMDA (*N*-methyl-ᴅ-aspartate) receptor-dependent long-term potentiation (LTP) shapes neural circuits and mediates learning and memory. During the induction of NMDA-receptor-dependent LTP, Ca^{2+} influx stimulates recruitment of synaptic AMPA (α-amino-3-hydroxy-5-methyl-4-isoxazole propionic acid) receptors, thereby strengthening synapses. How Ca^{2+} induces the recruitment of AMPA receptors remains unclear. Here we show that, in the pyramidal neurons of the hippocampal CA1 region in mice, blocking postsynaptic expression of both synaptotagmin-1 (Syt1) and synaptotagmin-7 (Syt7), but not of either alone, abolished LTP. LTP was restored by expression of wild-type Syt7 but not of a Ca^{2+}-binding-deficient mutant Syt7. Blocking postsynaptic expression of Syt1 and Syt7 did not impair basal synaptic transmission, reduce levels of synaptic or extrasynaptic AMPA receptors, or alter other AMPA receptor trafficking events. Moreover, expression of dominant-negative mutant Syt1 which inhibits Ca^{2+}-dependent presynaptic vesicle exocytosis, also blocked Ca^{2+}-dependent postsynaptic AMPA receptor exocytosis, thereby abolishing LTP. Our results suggest that postsynaptic Syt1 and Syt7 act as redundant Ca^{2+}-sensors for Ca^{2+}-dependent exocytosis of AMPA receptors during LTP, and thereby delineate a simple mechanism for the recruitment of AMPA receptors that mediates LTP.

Synapses connect the neurons in the brain into vast communicating networks composed of overlapping circuits that are highly dynamic owing to synaptic plasticity. Arguably the most compelling form of such plasticity is NMDA receptor (NMDAR)-dependent LTP[1–3]. NMDAR-dependent LTP is crucial for the formation of neural circuits and for the restructuring of neural circuits during learning and memory[4]. NMDAR-dependent LTP operates widely in the brain, but has been most extensively studied at CA3–CA1 Schaffer collateral synapses in the hippocampus[1–3]. During LTP induction, coincident stimulation of presynaptic inputs on a postsynaptic neuron gates a postsynaptic influx of Ca^{2+} through NMDARs. Intracellular Ca^{2+} then causes an increase in postsynaptic levels of AMPA receptors (AMPARs), thereby enhancing synaptic strength[2,3]. The mechanisms that increase postsynaptic AMPAR levels during LTP are not completely understood, although it has been suggested that the Ca^{2+}-dependent capture of extrasynaptic AMPARs by postsynaptic specializations is the most critical step[5–7]. However, blocking postsynaptic membrane fusion impairs AMPAR recruitment during LTP[8–10], suggesting that Ca^{2+}-dependent AMPAR exocytosis is also involved. Thus, two major questions arise: what molecular mechanisms deliver AMPARs to synapses during LTP, and how are these mechanisms regulated by Ca^{2+}?

In considering these questions, we focused on the potential role of postsynaptic synaptotagmins in LTP because synaptotagmins are well established Ca^{2+} sensors for Ca^{2+}-triggered exocytosis[11], and because complexin, a co-factor for synaptotagmins in exocytosis[12,13], is also postsynaptically essential for LTP[9]. Among synaptotagmins, synaptotagmin-1 (Syt1) acts as the main Ca^{2+} sensor for fast presynaptic vesicle exocytosis, whereas synaptotagmin-7 (Syt7) functions as the predominant Ca^{2+} sensor for a slower form of exocytosis[14–17]. Moreover, Syt1 and Syt7 are redundantly essential for Ca^{2+}-stimulated chromaffin granule exocytosis, which exhibits a time course similar to

that of LTP induction[18]. Here, we show that Syt1 and Syt7 act as essential but redundant postsynaptic Ca^{2+} sensors for AMPAR exocytosis during LTP, uncovering a simple mechanism for the Ca^{2+}-dependent recruitment of AMPARs during LTP (Extended Data Fig. 1).

Postsynaptic Syt1–Syt7 loss blocks LTP

To examine the role of Syt1 and Syt7 in LTP, we applied well-characterized Syt1 and Syt7 short hairpin RNAs (shRNAs), which suppress expression of Syt1 and Syt7 by more than 80%[16,17,19] (Extended Data Fig. 2). Using stereotactic injections of adeno-associated viruses (AAVs) into juvenile mice, we expressed these shRNAs *in vivo* separately or together in the hippocampal CA1 region, and recorded whole-cell currents from individual pyramidal neurons in acute slices 20–36 days after injection (Fig. 1a). Neurons infected with control AAVs or with AAVs expressing only Syt1 or Syt7 shRNAs exhibited robust LTP (Fig. 1b). By contrast, neurons infected with AAVs expressing both Syt1 and Syt7 shRNAs (Syt1–Syt7 DKD) were, on average, unable to generate LTP (Fig. 1b and Extended Data Fig. 3a). We confirmed that LTP elicited by our standard induction protocol was blocked by the NMDAR antagonist 2-amino-5-phosphonovalerate (AP5) and by the calmodulin (CaM) kinase IIα inhibitor autocamtide-2-related inhibitor peptide (AIP; Extended Data Fig. 3b).

Next, we used stereotactic injections of lentiviruses that expressed Syt1 and Syt7 shRNAs with enhanced green fluorescent protein (eGFP). In contrast to AAVs, which infect nearly all neurons in a particular brain region, lentiviruses infect only a sparse subset of neurons (Fig. 1a). Strikingly, lentiviral expression of Syt1 and Syt7 shRNAs blocked LTP, demonstrating a cell-autonomous mechanism (Fig. 1c and Extended Data Fig. 3c).

To control for potential off-target effects caused by RNA interference (RNAi) knockdowns, we performed additional experiments. First,
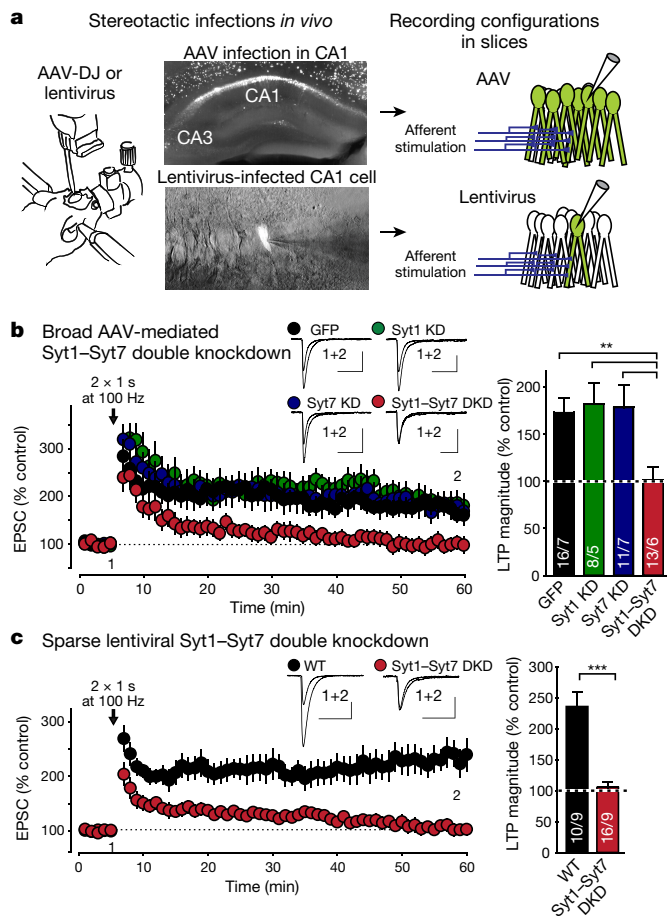
Figure 1 | Inhibiting postsynaptic expression of Syt1 and Syt7 blocks LTP by a cell-autonomous mechanism. a, Experimental strategy. Left, schematic of stereotactic virus injections; centre, representative eGFP fluorescence images of hippocampal slices after global AAV or sparse lentivirus infection; right, schematic of whole-cell recordings in acute slices. **b**, AAV-mediated double knockdown (DKD) of Syt1 and Syt7 suppresses NMDAR-dependent LTP. Left, representative traces and LTP time course; right, summary graphs of LTP magnitude. **c**, Same as **b**, but for sparse lentiviral double knockdown of Syt1 and Syt7. Data are mean ± s.e.m. (numbers in bars show number of neurons or mice analysed). Statistical significance was assessed by the Kruskal–Wallis test followed by the Mann–Whitney U test (**b**), or by the Mann–Whitney U test only (**c**; **$P < 0.01$; ***$P < 0.001$). In **b** and **c**, calibration bars are 50 pA, 50 ms.

lentiviral expression of an independent Syt7 shRNA[16] with Syt1 knockdown blocked LTP (Extended Data Fig. 3d). Second, the block of LTP by knockdowns of both Syt1 and Syt7 could be reversed by the expression of an shRNA-insensitive Syt7 rescue mRNA (Fig. 2a and Extended Data Fig. 3e). Third, mutations in the C2A-domain Ca^{2+}-binding sites of Syt7 (Syt7-C2A*), which impair its presynaptic function in neurotransmitter release[16,17], blocked the rescue of LTP, suggesting that binding of Ca^{2+} to Syt7 is essential for its function in LTP (Fig. 2b and Extended Data Fig. 3e). The same mutation had no effect on neurotransmitter release[16] or on LTP in wild-type neurons (Fig. 2b and Extended Data Fig. 3e), and is thus not dominant-negative. Fourth, lentiviral expression of Syt1 shRNA in constitutive Syt7 knockout mice (which exhibited normal LTP) also ablated LTP; again, LTP was rescued with wild-type Syt7 (Extended Data Fig. 3f). Fifth, postsynaptic deletion of Syt1 in double-mutant mice carrying homozygous Syt1 conditional and Syt7 constitutive knockout alleles[20] (Extended Data Fig. 3g–i) also robustly blocked LTP (Fig. 2c and Extended Data Fig. 3e).

NMDAR-dependent LTP is induced by Ca^{2+}-influx through NMDAR channels[1–3]. A similar form of LTP, termed voltage-pulse LTP, is elicited
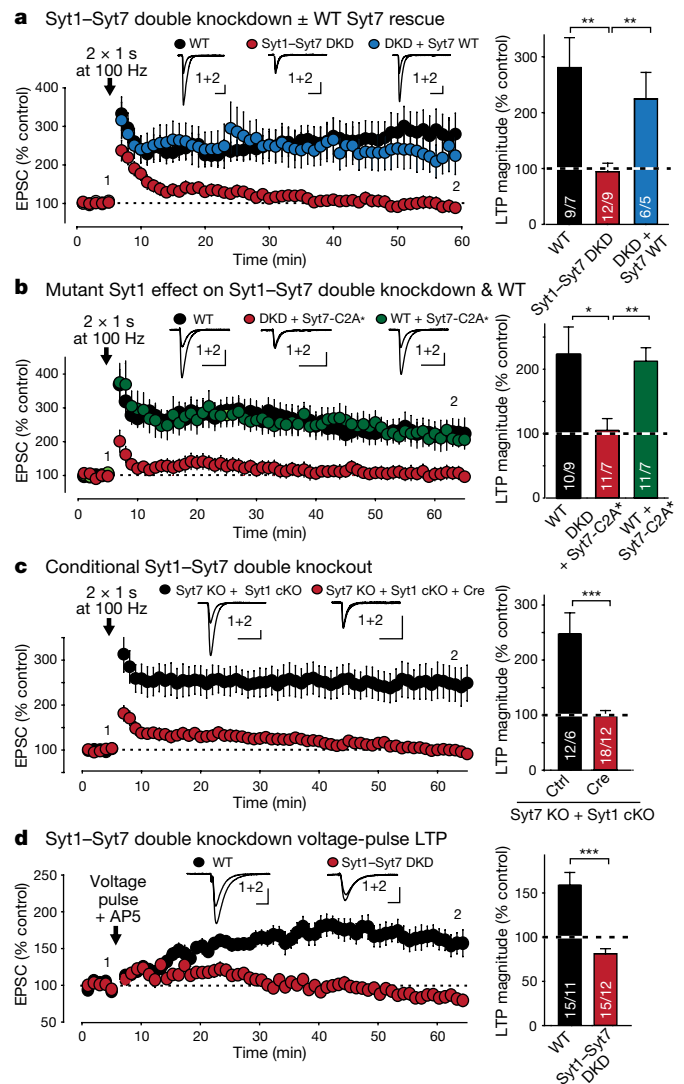

Figure 2 | Inhibiting postsynaptic Syt1 and Syt7 expression by various molecular manipulations blocks LTP. a, b, Block of LTP by the Syt1–Syt7 DKD was rescued by shRNA-resistant wild-type (**a**) but not mutant (**b**) Syt7 (Syt7-C2A* contains inactivated C2A-domain Ca^{2+}-binding sites). Left, representative traces and LTP time course; right, summary graphs of LTP magnitude. **c**, Conditional knockout (cKO) of postsynaptic Syt1 in constitutive Syt7 knockout mice blocks LTP. **d**, Postsynaptic Syt1–Syt7 DKD also blocks LTP induced by depolarizing voltage pulses in the presence of the NMDAR antagonist AP5 (50 μM). Data are mean ± s.e.m. (numbers in bars are number of neurons or mice analysed). Statistical significance was assessed using the Kruskal–Wallis test followed by pairwise comparisons with the Mann–Whitney U test (**a, b**), or simply by the Mann–Whitney U test (**c, d**; *$P < 0.05$; **$P < 0.01$; ***$P < 0.001$). Calibration bars: 50 pA, 50 ms for **a–c**; 50 pA, 10 ms for **d**.

by gating postsynaptic Ca^{2+}-influx via L-type Ca^{2+}-channels during blockade of NMDARs[21,22]. Thus, voltage-pulse LTP is independent of presynaptic neurotransmitter release or postsynaptic NMDARs. Notably, voltage-pulse LTP was also abolished by postsynaptic ablation of Syt1 and Syt7, similar to NMDAR-dependent LTP (Fig. 2d and Extended Data Fig. 3e).

Together these data show that inhibition of postsynaptic Syt1 and Syt7 expression blocks LTP induced by postsynaptic increases in Ca^{2+}, independent of the source of Ca^{2+}. The postsynaptic Ca^{2+}-dependent function of Syt1 and Syt7 is surprising given the abundant presynaptic localization of Syt1 and Syt7 (ref. 11). Although most Syt1 and Syt7 is presynaptic, postsynaptic dendritic Syt1 and Syt7 can be detected (Extended Data Fig. 4). Moreover, double-knockout neurons lacking
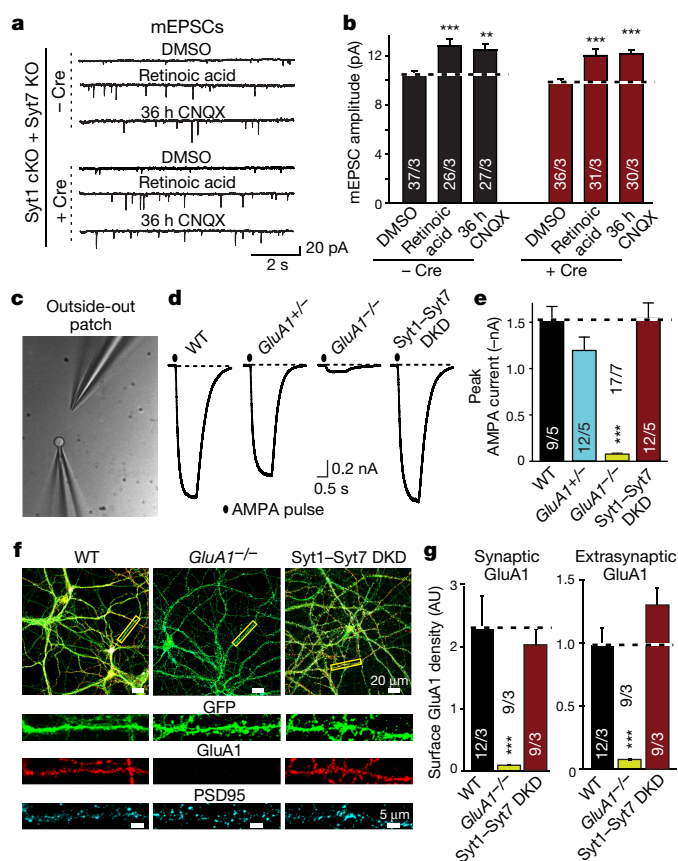
Figure 3 | Postsynaptic Syt1–Syt7 deficiency does not decrease AMPAR recruitment during homeostatic plasticity or surface AMPAR levels.
a, **b**, Syt1–Syt7 DKO does not impair AMPAR exocytosis induced in cultured hippocampal slices by chronic synaptic silencing with CNQX (36 h) or by acute application of retinoic acid (4 h). **c**, Phase-contrast image of a patch pipette with a nucleated outside-out patch (bottom) and an AMPA-puffing pipette (top). **d**, Representative traces of currents induced by the active enantiomer of AMPA, s-AMPA (10 μM for 1 s) in outside-out patches. **e**, Summary graph of the mean AMPA-puff-induced peak current amplitude. **f**, Representative images of control (wild-type), GluA1 knockout ($GluA1^{-/-}$, also known as $Gria1^{-/-}$) and Syt1–Syt7 double knockout hippocampal neurons that express eGFP (green) and were stained for surface GluA1 receptors (red) and cytoplasmic PSD95 (cyan). **g**, Summary graphs of surface GluA1 staining intensity per pixel in synaptic (signal coincident with PSD95) and extrasynaptic membranes (signal non-coincident with PSD95). AU, arbitrary units. Data are mean ± s.e.m. (numbers in bars show number of neurons and mice analysed). Statistical significance was assessed with the Kruskal–Wallis test followed by pairwise comparisons with the Mann–Whitney U test (**$P < 0.01$; ***$P < 0.001$).

Syt3 and Syt5—which belong to a different class of synaptotagmins[11] and are the only other two Ca^{2+}-binding synaptotagmins that are abundantly expressed in CA1 pyramidal neurons—exhibited no impairment of LTP (Extended Data Fig. 5a), demonstrating that the block of LTP by inhibition of postsynaptic Syt1 and Syt7 expression is specific to these synaptotagmins.

Syt1 and Syt7 in other AMPAR trafficking events
Although our results suggest that Syt1 and Syt7 are redundantly essential for AMPAR exocytosis during LTP, alternative explanations are possible. Brain-derived neurotrophic factor (BDNF) may play an instructive role in synaptic plasticity[23,24], prompting us to investigate whether the Syt1 and Syt7 double deficiency blocked LTP by inhibiting BDNF secretion. However, BDNF application did not reverse the phenotype, arguing against this explanation (Extended Data Fig. 5b).

Another possible explanation for the Syt1 and Syt7 requirement in LTP is that depletion of Syt1 and Syt7 might decrease basal synaptic strength, although this would not explain the loss of voltage-pulse-induced LTP. However, we observed no differences in basal AMPAR or NMDAR excitatory postsynaptic currents (EPSCs) between control and Syt1–Syt7 DKD neurons during dual patch-clamp recordings of adjacent control and Syt1–Syt7 DKD pyramidal CA1 neurons (Extended Data Fig. 6a–d). Moreover, we observed no major differences between control and Syt1–Syt7 DKD neurons in the paired-pulse ratio (PPR) of AMPAR EPSCs (Extended Data Fig. 6e) or in the properties of spontaneous miniature excitatory postsynaptic currents (mEPSCs) (Extended Data Fig. 6f–h). Thus, postsynaptic loss of Syt1and Syt7 function does not change basal synaptic transmission at synapses on affected neurons.

Next, we assessed whether other forms of synaptic plasticity involving AMPAR trafficking were impaired by the Syt1–Syt7 double deficiency. Homeostatic plasticity induced by chronic synaptic silencing (36-h application of 6-cyano-7-nitroquinoxaline-2,3-dione (CNQX)) or by direct application of retinoic acid (4-h application) potently stimulates synaptic AMPAR recruitment[25]. Loss of Syt1 and Syt7 had no effect on either form of synaptic AMPAR recruitment (Fig. 3a, b and Extended Data Fig. 7a–d), demonstrating that Syt1 and Syt7 are essential specifically for Ca^{2+}-induced AMPAR recruitment during LTP. Similarly, we observed no effect of the Syt1–Syt7 double deficiency on postsynaptic long-term depression (LTD), which involves NMDAR-dependent AMPAR endocytosis[2,3,26] (Extended Data Fig. 7e). Thus, postsynaptic loss of Syt1 and Syt7 in CA1 pyramidal neurons did not impair the activity-dependent trafficking of AMPARs, as far as measured, except during LTP.

Extrasynaptic AMPARs
As a further alternative explanation of our results, we investigated whether the postsynaptic Syt1–Syt7 deficiency could block LTP by reducing delivery of extrasynaptic AMPARs without decreasing synaptic AMPARs, as observed after genetic deletion of the AMPAR subunit GluA1 (encoded by $Gria1$)[7,27]. To test this hypothesis, we pulled nucleated somatic outside-out patches from CA1 neurons in acute slices, and measured currents induced by application of AMPA (Fig. 3c, d). We observed no change in AMPA-induced currents in Syt1–Syt7 DKD neurons, but, as expected, detected a massive decrease in these currents in homozygous GluA1 knockout neurons[7,27] (Fig. 3e and Extended Data Fig. 8a, b). Moreover, we analysed immunocytochemical staining of surface GluA1 in cultured Syt1–Syt7 DKD hippocampal neurons, using wild-type and GluA1 knockout neurons as controls (Fig. 3f). Syt1–Syt7 double-deficient neurons again exhibited no detectable change in extrasynaptic or synaptic surface GluA1 (as defined by co-localization with the postsynaptic density protein PSD95), whereas, again as expected, GluA1 knockout neurons displayed a large decrease in surface GluA1 receptors (Fig. 3g). Thus, two complementary assays demonstrate that the postsynaptic Syt1–Syt7 deficiency did not cause a decrease in extrasynaptic AMPARs.

The normal levels of synaptic and extrasynaptic AMPARs in Syt1–Syt7 DKD neurons show that either constitutive AMPAR exocytosis and endocytosis are normal, or AMPAR exocytosis and endocytosis are both changed in parallel. To investigate the latter possibility, we analysed the effect of the Syt1–Syt7 double deficiency on the constitutive endocytosis of AMPARs, but detected no significant change (Extended Data Fig. 8c–e). Thus, constitutive AMPAR trafficking overall was likely to be normal.

Syt1–Syt7 loss impairs AMPAR exocytosis
To further assess whether the Syt1–Syt7 double deficiency blocked LTP-induced, Ca^{2+}-triggered AMPAR exocytosis, we directly measured AMPAR exocytosis elicited by NMDAR activation in cultured hippocampal neurons, using a well-established chemical LTP (cLTP) protocol[28,29]. Induction of cLTP efficiently increased GluA1 surface levels in control neurons but not in Syt1–Syt7 DKD neurons (Fig. 4a, b), confirming that the Syt1–Syt7 deficiency impairs AMPAR exocytosis induced
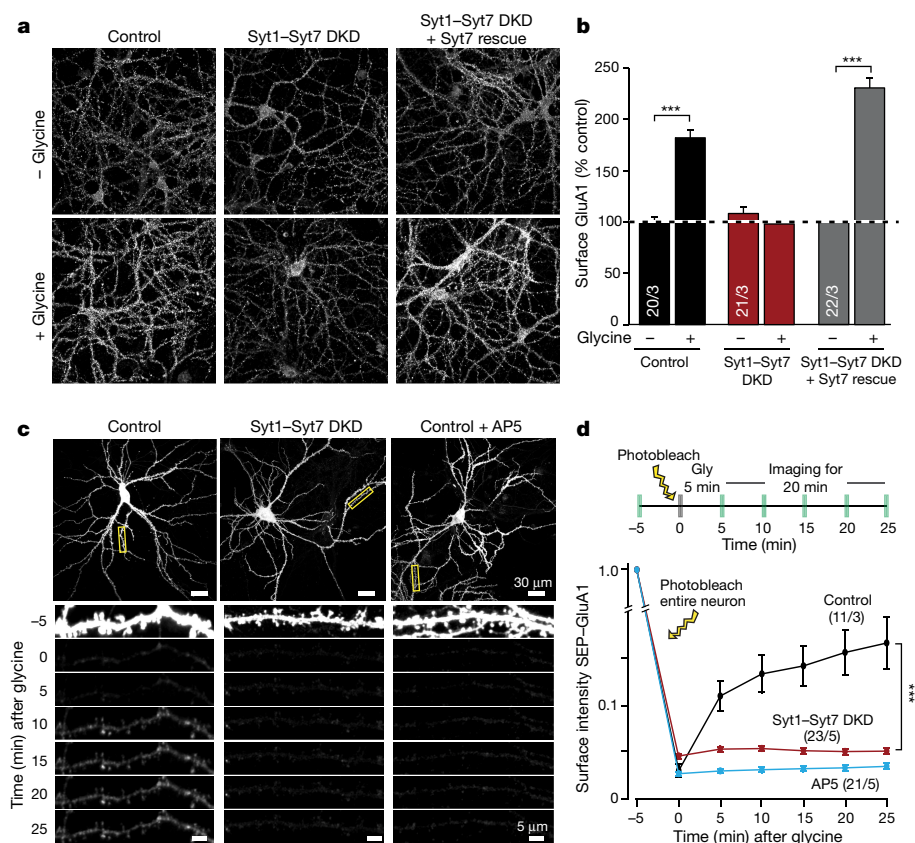
Figure 4 | Syt1–Syt7 deficiency blocks AMPAR exocytosis during 'chemical LTP' in cultured hippocampal neurons. a, b, Representative images (**a**) and summary graphs (**b**) of GluA1 surface immunostaining as a function of chemical LTP (cLTP) induced by glycine. **c, d,** Representative images (**c**) and summary graph (**d**) of live-cell SEP–GluA1 fluorescence in hippocampal control neurons expressing transfected SEP–GluA1, imaged before and after cLTP induction with glycine. Data in **b** and **d** are mean ± s.e.m. (numbers in bars show number of neurons and independent cultures analysed). Statistical significance was assessed by the Mann–Whitney U test (**b**; ***$P < 0.001$) or by two-way ANOVA (**d**; ***$P < 0.001$).

by NMDAR activation. Again, the block of cLTP in neurons lacking Syt1 and Syt7 was reversed by expression of wild-type Syt7 (Fig. 4a, b).

It is possible that the NMDAR-dependent increase in surface GluA1 during cLTP could be due to clustering of pre-existing, diffuse surface GluA1-containing AMPARs, rendering them more detectable by immunocytochemistry, and thus that the Syt1–Syt7 deficiency impairs AMPAR clustering instead of AMPAR exocytosis. To directly test this possibility, we visualized AMPAR exocytosis in real time by combining cLTP with live-cell imaging of neurons overexpressing SEP–GluA1[30,31]. In SEP–GluA1, the extracellular N terminus of GluA1 is fused with a supereliptic pHluorin (SEP), a pH-sensitive GFP that becomes fluorescent when exposed to the extracellular milieu, but not when it is within an acidic intracellular trafficking vesicle. To eliminate the possibility that cLTP increased detection of pre-existing surface SEP–GluA1 owing to clustering, we photobleached all surface SEP–GluA1 before inducing cLTP (Fig. 4c, d). In control cells, subsequent cLTP induction significantly increased SEP–GluA1 fluorescence during the 25-min duration of our experiment; this increase was blocked by the NMDAR antagonist AP5 (Fig. 4c, d). Notably, the Syt–Syt7 deficiency almost abolished this increase (Fig. 4c, d). Thus, Syt1 and Syt7 are redundantly required for NMDAR-induced AMPAR exocytosis.

Probing Ca²⁺-triggered exocytosis

Do Syt1 and Syt7 function in postsynaptic AMPAR exocytosis as actual Ca^{2+} sensors, or as Ca^{2+}-independent trafficking proteins? This question arises because in presynaptic vesicle exocytosis, Syt1 and Syt7 act both as Ca^{2+} sensors and as priming factors[11,14–17]. The lack of LTP rescue by the Ca^{2+}-binding mutant Syt7-C2A* supports the Ca^{2+} sensor hypothesis (Fig. 2b). To further test this conclusion, we sought to develop tools that could differentiate between the priming and Ca^{2+}-sensing functions of synaptotagmins.

In *Drosophila*, Ca^{2+}-binding site mutants of Syt1 are dominant-negative inhibitors of neurotransmitter release[32]. We asked whether the same was true in mammals using mutant Syt1 with inactivating substitutions in the Ca^{2+}-binding sites of the C2A (Syt1-C2A*) or C2B

domain (Syt1-C2B*), or of both (Syt1-C2A*B*). In cultured wild-type hippocampal neurons, Syt1-C2B* robustly inhibited release, whereas Syt1-C2A* had no effect (Fig. 5a, b and Extended Data Fig. 9a). The Syt1-C2A*B* double mutation enhanced the dominant-negative inhibition of release by the Syt1-C2B* single mutation, suggesting that both C2 domains contribute to this process (Fig. 5a, b). Syt1-C2A*B* blocked release at both excitatory and inhibitory synapses (Fig. 5a, b and Extended Data Fig. 9a, c). The Syt1 mutants, however, did not impair Ca^{2+}-independent vesicle exocytosis induced by hypertonic sucrose, which stimulates Ca^{2+}-independent exocytosis of all primed synaptic vesicles[33] (Fig. 5a, c and Extended Data Fig. 9b).

Strikingly, dominant-negative Syt1-C2A*B* suppressed not only synchronous release in wild-type synapses, but also asynchronous release, which remains in Syt1 knockout neurons and is ablated by the additional deletion of Syt7[16] (Fig. 5d). Thus, Syt1-C2A*B* blocked both Syt1 and Syt7 function. However, inhibiting Syt7 expression in Syt1 knockout neurons additionally decreased Ca^{2+}-independent release induced by hypertonic sucrose[17], whereas dominant-negative Syt1-C2A*B* had no effect on sucrose-induced release in Syt1 knockout neurons (Fig. 5e). Thus, Syt1-C2A*B* is a dominant-negative inhibitor of Ca^{2+}-dependent but not of Ca^{2+}-independent synaptotagmin function, making it a suitable tool for understanding the role of Syt1 and Syt7 in regulated AMPAR exocytosis.

Syt1–C2A*B* blocks LTP

We sparsely expressed dominant-negative Syt1-C2A*B* in CA1 wild-type neurons *in vivo*, and measured NMDAR-dependent LTP and voltage-pulse-induced LTP in acute slices. Syt1-C2A*B* potently blocked both forms of LTP (Fig. 5f), but had no notable effect on the parameters of basal excitatory synaptic transmission, such as PPR, AMPAR/NMDAR ratio, mEPSC frequency and mEPSC amplitude (Extended Data Fig. 9d–h).

These results indicate that Syt1 and Syt7 perform an essential Ca^{2+} sensor function in AMPAR exocytosis during LTP. To test this conclusion independently with yet another approach, we examined
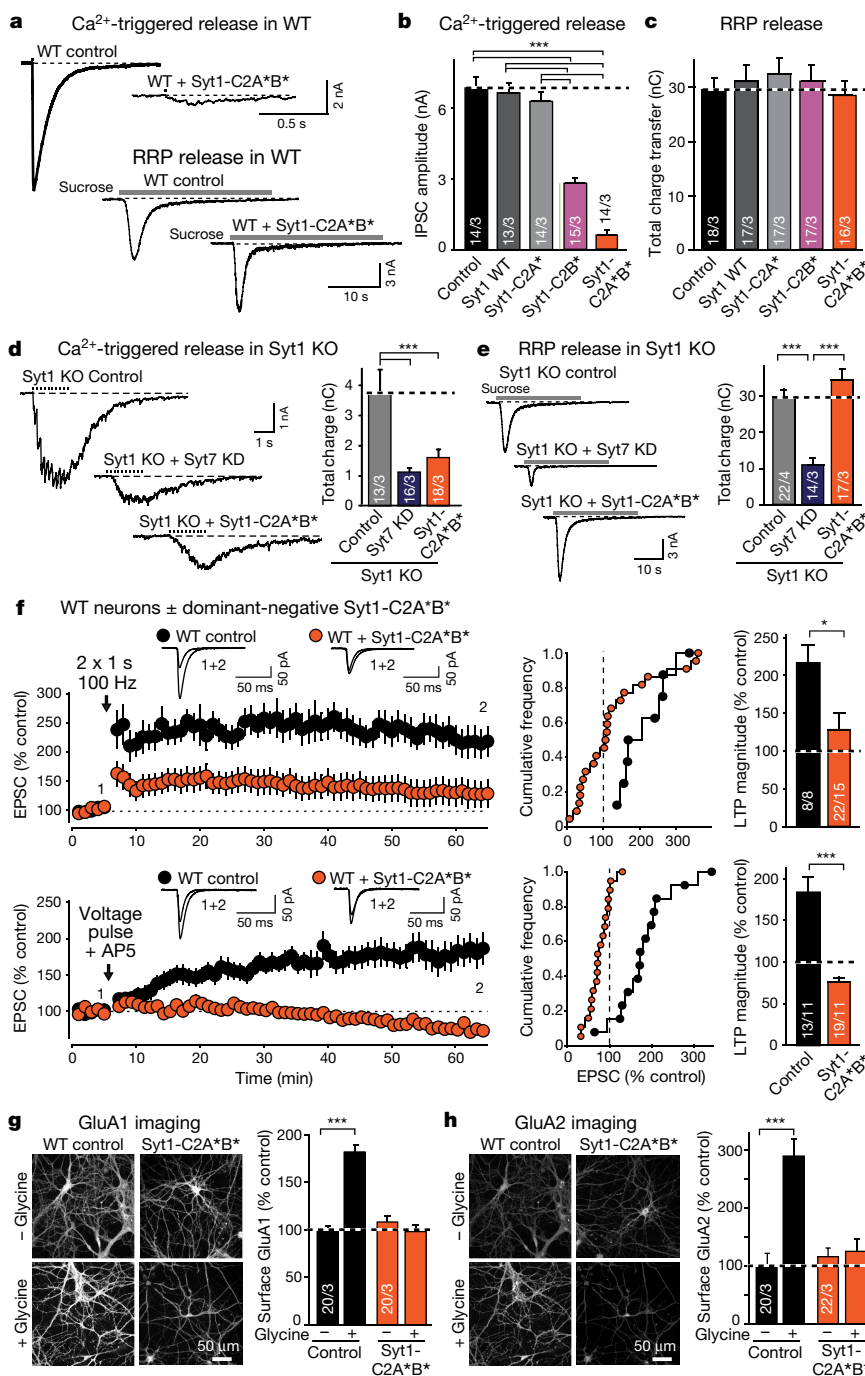
Figure 5 | Dominant-negative mutant Syt1 impairs presynaptic Ca²⁺-induced vesicle exocytosis and postsynaptic LTP-induced AMPAR exocytosis. a–c, Effect of Syt1 with Ca²⁺-binding site mutations in the C2A domain (Syt1-C2A*), the C2B domain (Syt1-C2B*) or both (Syt1C2A*B*) on inhibitory postsynaptic currents (IPSCs) triggered by action potentials or by hypertonic sucrose in cultured hippocampal wild-type neurons (**a**, representative traces; **b**, **c**, summary graphs; for more data, see Extended Data Fig. 9a–c). **d, e**, Comparative effects of the Syt7 knockdown and the dominant-negative Syt1-C2A*B* mutant on asynchronous IPSCs induced by a 1-s, 10-Hz stimulus train (**d**) or a 30-s application of 0.5 M sucrose (**e**) in cultured hippocampal Syt1-knockout neurons. **f**, Dominant-negative Syt1-C2A*B*

mutant suppresses LTP in acute hippocampal slices (top, NMDAR-dependent LTP; bottom, voltage-pulse LTP in the presence of 50 μM AP5). Experiments were performed as for Figs 1 and 2. **g, h**, Dominant-negative Syt1-C2A*B* suppresses cLTP in cultured wild-type hippocampal neurons. Representative images (left) and summary graphs (right) of neurons without or with glycine induction of cLTP, surface-labelled for GluA1 (**g**) or GluA2 (**h**). Data are mean ± s.e.m. (numbers in bars show number of neurons and independent cultures or neurons and mice analysed). Statistical significance was assessed by the Kruskal–Wallis test followed by the Mann–Whitney U test (**b–e**; ***P < 0.001) or the Mann–Whitney U test only (**f–h**; *P < 0.05; ***P < 0.001).

the effect of dominant-negative Syt1-C2A*B* in cultured wild-type hippocampal neurons on cLTP, and monitored surface levels of both GluA1 and GluA2 (Fig. 5g, h). As expected, induction of cLTP greatly increased surface levels of both GluA1 and GluA2 in control neurons. In marked contrast, dominant-negative Syt1-C2A*B* completely

blocked the increases in surface GluA1 and GluA2 during cLTP, but had no effect on steady-state surface levels of GluA1 or GluA2 (Fig. 5g, h). Thus, selectively blocking the Ca²⁺ sensor function of Syt1 and Syt7 using dominant-negative Syt1-C2A*B* blocked LTP-induced AMPAR exocytosis in slices and in cultured neurons.

Summary

Using multiple *in vivo* and *in vitro* manipulations of postsynaptic Syt1 and Syt7, we show that NMDAR-dependent LTP requires Syt1 or Syt7 as functionally redundant Ca^{2+} sensors for AMPAR exocytosis (Extended Data Figs 1, 10). Our results imply that Ca^{2+}-triggered AMPAR exocytosis is a critical step in LTP and that Ca^{2+}-regulated membrane traffic is governed by similar mechanisms in presynaptic and postsynaptic compartments, revealing an unexpectedly economical organization of synapses. Two independent lines of evidence directly show that Syt1 and Syt7 act as Ca^{2+} sensors for AMPAR exocytosis during LTP. First, a mutation in Syt7 that abolishes Ca^{2+} binding but does not produce a dominant-negative effect fails to rescue LTP (Fig. 2b). Second, a mutation in Syt1 that abolishes Ca^{2+} binding and renders it dominant-negative for Ca^{2+} sensing but not for Ca^{2+}-independent exocytosis also blocks LTP (Fig. 5). CaM kinase $II\alpha$, which is activated by Ca^{2+}, is also essential for LTP[34–36], raising the question of how Ca^{2+}-sensing by synaptotagmins and CaM kinase $II\alpha$ work together in LTP. Several mechanisms are conceivable; for example, CaM kinase $II\alpha$ might activate exocytosis, possibly through phosphorylation of Syt1 and Syt7[37,38], or CaM kinase $II\alpha$ may play a role in stably capturing AMPARs in postsynaptic sites[39,40]. It seems likely that Ca^{2+}-induced AMPAR exocytosis during LTP is perisynaptic, with subsequent lateral diffusion of perisynaptic AMPARs into the postsynaptic density[3,5,6], but direct exocytosis of AMPAR vesicles into the postsynaptic membrane cannot at present be ruled out.

The unexpected discovery of a critical role of postsynaptic synaptotagmins as Ca^{2+}-sensors for LTP provides new insight into synaptic plasticity. Showing that presynaptic and postsynaptic mechanisms share critical features renders LTP a simple and economical process, as would be expected for a universal mechanism involved in circuit plasticity.

1. Bliss, T. V. & Collingridge, G. L. A synaptic model of memory: long-term potentiation in the hippocampus. *Nature* **361,** 31–39 (1993).
2. Malenka, R. C. & Bear, M. F. LTP and LTD: an embarrassment of riches. *Neuron* **44,** 5–21 (2004).
3. Huganir, R. L. & Nicoll, R. A. AMPARs and synaptic plasticity: the last 25 years. *Neuron* **80,** 704–717 (2013).
4. Morris, R. G. NMDA receptors and memory encoding. *Neuropharmacology* **74,** 32–40 (2013).
5. Opazo, P. & Choquet, D. A three-step model for the synaptic recruitment of AMPA receptors. *Mol. Cell. Neurosci.* **46,** 1–8 (2011).
6. Makino, H. & Malinow, R. AMPA receptor incorporation into synapses during LTP: the role of lateral movement and exocytosis. *Neuron* **64,** 381–390 (2009).
7. Granger, A. J., Shi, Y., Lu, W., Cerpas, M. & Nicoll, R. A. LTP requires a reserve pool of glutamate receptors independent of subunit type. *Nature* **493,** 495–500 (2013).
8. Lledo, P. M., Zhang, X., Südhof, T. C., Malenka, R. C. & Nicoll, R. A. Postsynaptic membrane fusion and long-term potentiation. *Science* **279,** 399–403 (1998).
9. Ahmad, M. *et al.* Postsynaptic complexin controls AMPA receptor exocytosis during LTP. *Neuron* **73,** 260–267 (2012).
10. Jurado, S. *et al.* LTP requires a unique postsynaptic SNARE fusion machinery. *Neuron* **77,** 542–558 (2013).
11. Südhof, T. C. Neurotransmitter release: the last millisecond in the life of a synaptic vesicle. *Neuron* **80,** 675–690 (2013).
12. Reim, K. *et al.* Complexins regulate the Ca^{2+} sensitivity of the synaptic neurotransmitter release machinery. *Cell* **104,** 71–81 (2001).
13. Maximov, A., Tang, J., Yang, X., Pang, Z. P. & Südhof, T. C. Complexin controls the force transfer from SNARE complexes to membranes in fusion. *Science* **323,** 516–521 (2009).
14. Geppert, M. *et al.* Synaptotagmin I: a major Ca^{2+} sensor for transmitter release at a central synapse. *Cell* **79,** 717–727 (1994).
15. Wen, H. *et al.* Distinct roles for two synaptotagmin isoforms in synchronous and asynchronous transmitter release at zebrafish neuromuscular junction. *Proc. Natl Acad. Sci. USA* **107,** 13906–13911 (2010).
16. Bacaj, T. *et al.* Synaptotagmin-1 and synaptotagmin-7 trigger synchronous and asynchronous phases of neurotransmitter release. *Neuron* **80,** 947–959 (2013).
17. Bacaj, T. *et al.* Synaptotagmin-1 and -7 are redundantly essential for maintaining the capacity of the readily-releasable pool of synaptic vesicles. *PLoS Biol.* **13,** e1002267 (2015).
18. Schonn, J. S., Maximov, A., Lao, Y., Südhof, T. C. & Sørensen, J. B. Synaptotagmin-1 and -7 are functionally overlapping Ca^{2+} sensors for exocytosis in adrenal chromaffin cells. *Proc. Natl Acad. Sci. USA* **105,** 3998–4003 (2008).
19. Xu, W. *et al.* Distinct neuronal coding schemes in memory revealed by selective erasure of fast synchronous synaptic transmission. *Neuron* **73,** 990–1001 (2012).
20. Zhou, Q. *et al.* Architecture of the synaptotagmin–SNARE machinery for neuronal exocytosis. *Nature* **525,** 62–67 (2015).
21. Wyllie, D. J., Manabe, T. & Nicoll, R. A. A rise in postsynaptic Ca^{2+} potentiates miniature excitatory postsynaptic currents and AMPA responses in hippocampal neurons. *Neuron* **12,** 127–138 (1994).
22. Kato, H. K., Watabe, A. M. & Manabe, T. Non-Hebbian synaptic plasticity induced by repetitive postsynaptic action potentials. *J. Neurosci.* **29,** 11153–11160 (2009).
23. Kang, H. & Schuman, E. M. Long-lasting neurotrophin-induced enhancement of synaptic transmission in the adult hippocampus. *Science* **267,** 1658–1662 (1995).
24. Harward, S. C. *et al.* Autocrine BDNF-TrkB signalling within a single dendritic spine. *Nature* **538,** 99–103 (2016).
25. Arendt, K. L. *et al.* Calcineurin mediates homeostatic synaptic plasticity by regulating retinoic acid synthesis. *Proc. Natl Acad. Sci. USA* **112,** E5744–E5752 (2015).
26. Dudek, S. M. & Bear, M. F. Homosynaptic long-term depression in area CA1 of hippocampus and effects of N-methyl-D-aspartate receptor blockade. *Proc. Natl Acad. Sci. USA* **89,** 4363–4367 (1992).
27. Zamanillo, D. *et al.* Importance of AMPA receptors for hippocampal synaptic plasticity but not for spatial learning. *Science* **284,** 1805–1811 (1999).
28. Lu, W. *et al.* Activation of synaptic NMDA receptors induces membrane insertion of new AMPA receptors and LTP in cultured hippocampal neurons. *Neuron* **29,** 243–254 (2001).
29. Passafaro, M., Piëch, V. & Sheng, M. Subunit-specific temporal and spatial patterns of AMPA receptor exocytosis in hippocampal neurons. *Nat. Neurosci.* **4,** 917–926 (2001).
30. Lin, D. T. & Huganir, R. L. PICK1 and phosphorylation of the glutamate receptor 2 (GluR2) AMPA receptor subunit regulates GluR2 recycling after NMDA receptor-induced internalization. *J. Neurosci.* **27,** 13903–13908 (2007).
31. Kwon, O. B., Longart, M., Vullhorst, D., Hoffman, D. A. & Buonanno, A. Neuregulin-1 reverses long-term potentiation at CA1 hippocampal synapses. *J. Neurosci.* **25,** 9378–9383 (2005).
32. Lee, J., Guan, Z., Akbergenova, Y. & Littleton, J. T. Genetic analysis of synaptotagmin C2 domain specificity in regulating spontaneous and evoked neurotransmitter release. *J. Neurosci.* **33,** 187–200 (2013).
33. Rosenmund, C. & Stevens, C. F. Definition of the readily releasable pool of vesicles at hippocampal synapses. *Neuron* **16,** 1197–1207 (1996).
34. Malinow, R., Schulman, H. & Tsien, R. W. Inhibition of postsynaptic PKC or CaMKII blocks induction but not expression of LTP. *Science* **245,** 862–866 (1989).
35. Malenka, R. C. *et al.* An essential role for postsynaptic calmodulin and protein kinase activity in long-term potentiation. *Nature* **340,** 554–557 (1989).
36. Silva, A. J., Stevens, C. F., Tonegawa, S. & Wang, Y. Deficient hippocampal long-term potentiation in α-calcium-calmodulin kinase II mutant mice. *Science* **257,** 201–206 (1992).
37. Thiagarajan, T. C., Piedras-Renteria, E. S. & Tsien, R. W. α- and βCaMKII. Inverse regulation by neuronal activity and opposing effects on synaptic strength. *Neuron* **36,** 1103–1114 (2002).
38. Pang, Z. P., Cao, P., Xu, W. & Südhof, T. C. Calmodulin controls synaptic strength via presynaptic activation of calmodulin kinase II. *J. Neurosci.* **30,** 4132–4142 (2010).
39. Chetkovich, D. M., Chen, L., Stocker, T. J., Nicoll, R. A. & Bredt, D. S. Phosphorylation of the postsynaptic density-95 (PSD-95)/discs large/zona occludens-1 binding site of stargazin regulates binding to PSD-95 and synaptic targeting of AMPA receptors. *J. Neurosci.* **22,** 5791–5796 (2002).
40. Opazo, P. *et al.* CaMKII triggers the diffusional trapping of surface AMPARs through phosphorylation of stargazin. *Neuron* **67,** 239–252 (2010).

METHODS

No statistical methods were used to predetermine sample size. Experiments described in Figs 1b, 4, 5a–e, g, h and Extended Data Figs 3f, 5a, 8, 9a–c were randomized and investigators were blinded to allocation and outcome assessments; all other experiments were not randomized and investigators were not blinded.

Mice. Juvenile (P18–22) male mice (CD1 or CD1/Bl6/Sv129 hybrid strains) were used for all LTP experiments, and newborn male and female mice (same strains) for all culture experiments. All mouse lines used here (CD1, Syt7 knockout (KO), Syt1 conditional (c)KO, GluA1 KO, Syt1 KO, Nrxn1–HA knockin) except for 7SF (which is a new constitutive Syt7 KO line; see Extended Data Fig. 3g–i) have been described previously[14,16,20,27]. Experiments in Figs 2c, 3a, b and Extended Data Fig. 7a–d used 7SF; experiments in Extended Data Fig. 3f used our previously reported Syt7 KO mice. Mice were bred using standard procedures; all genetic strains have been deposited at Jackson Labs. All animal experiments were evaluated and approved by the Stanford University Administrative Panel on Laboratory Animal Care.

Plasmid constructs and viruses. An overview of the plasmids used is present in Extended Data Fig. 2. All plasmids, including the Syt1 and Syt7 knockdown lentiviral vectors used have been described previously[16,17,19,20]. The following oligonucleotide sequences were used for knockdowns: Syt7 KD606 AAAGACAAGCGGGTAGAGAAA; KD607 GATCTACCTGTCCTGGAAGAG; Syt1 GAGCAAATCCAGAAAGTGCAA. AAV-DJ viruses and lentiviruses were prepared as described[16,17,19].

The Syt7 Ca^{2+}-binding site mutant Syt7-C2A* contains the following mutations: D225A, D227A and D233A ref. 41. The Syt1 Ca^{2+}-binding site mutants contain the following mutations: Syt1-C2A*, D178A, D230A and D232A; Syt1-C2B*, D309A, D363A and D365A; Syt1-C2A*B*, a combination of all Syt1 mutations[42].

In vivo stereotactic injections. Mice (male, aged postnatal day (P)18–P22; weight 8–12 g) were anaesthetized with a mixture of ketamine (75 mg per kg body weight) and dexmedetomidine (0.375 mg per kg body weight) by intraperitoneal injection. Mice were immobilized on a Kopf stereotaxic apparatus and small bilateral holes were drilled into the skull at −1.8 mm posterior and −1.5 mm lateral to bregma for injection into the hippocampal CA1 region. Glass cannulae filled with viral solution were lowered to a depth of 1.35 mm (from the dura), and viral medium (0.6 μl) was injected using a microinjection pump (Harvard Apparatus) at a flow rate of 0.1 μl per min sequentially into each hemisphere. The scalp was then sealed and atipamezole (10 mg per kg body weight) was injected by intraperitoneal injection to reverse the effect of dexmedetomidine. Animals were monitored as they recovered from anaesthesia.

Acute slice electrophysiology. Mice were anaesthetized with isoflurane 20–36 days after in vivo virus injections. Their brains were then rapidly removed and placed in ice-cold, high-sucrose cutting solution containing (in mM): 75 sucrose, 85 NaCl, 24 NaHCO₃, 25 glucose, 2.5 KCl, 1.25 NaH₂PO₄, 4 MgCl₂ and 0.5 CaCl₂. Slices were sectioned on a Leica vibratome in high-sucrose cutting solution, and immediately transferred to an incubation chamber with artificial cerebrospinal fluid (ACSF) containing (in mM): 117.5 NaCl, 26.2 NaHCO₃, 11.0 glucose, 2.5 KCl, 1 NaH₂PO₄, 1.3 MgSO₄ and 2.5 CaCl₂. Slices were allowed to recover at 32 °C for 30 min before equilibration at room temperature for another hour. During recordings, slices were placed in a recording chamber perfused with heated ACSF (28–30 °C) and gassed continuously with 95% O_2 and 5% CO_2. All slice recordings were obtained with picrotoxin (50 μM) in the ACSF. Whole-cell recording pipettes (3–4 MΩ) were filled with a solution containing (in mM): 135 CsMeSO₄, 8 NaCl, 10 HEPES-NaOH pH 7.3, 0.25 EGTA, 2 MgCl₂, 4 Mg₂ATP, 0.3 Na₃GTP and 5 phosphocreatine (osmolarity 300). Data were collected with a MultiClamp 700B amplifier (Molecular Devices), digitized at 10 kHz using the Digidata 1322A data acquisition system (Molecular Devices) and analysed using a custom program written with Igor Pro software (Wavemetrics) or Clampex/Clampfit (Molecular Devices). The frequency, duration and magnitude of the extracellular stimulus were controlled with a Model 2100 Isolated Pulse Stimulator (A-M Systems). Evoked synaptic responses were triggered with a bipolar electrode.

LTP, voltage-pulse LTP and LTD. CA1 pyramidal cells were visualized by infrared differential interference contrast (DIC) imaging and GFP-positive neurons were identified by epifluorescence. A bipolar stimulation electrode was placed in the stratum radiatum to evoke EPSCs in CA1 pyramidal cells. Cells were held at −70 mV to record AMPAR EPSCs while stimulating afferent inputs at 0.1 Hz. LTP was induced by two trains of high-frequency stimulation (100 Hz, 1 s) separated by 20 s with the patched cells depolarized to −10 mV. This induction protocol was always applied within 10 min of achieving whole-cell configuration to avoid 'washout' of LTP. For voltage-pulse LTP, cells were depolarized 20 times from −70 mV to +10 mV for 1 s in the absence of stimulation but in the presence of AP5. To induce LTD, cells were held at −45 mV and one train of low frequency stimulation (1 Hz, 400 s) was applied. To generate summary graphs, individual experiments

were normalized to the baseline and six consecutive responses were averaged to generate 1-min bins. These were then averaged again to generate the final summary graphs. The magnitudes of LTP and LTD were calculated on basis of the averaged EPSC values during the last 5 min of the LTP and LTD summary graphs.

Dual cell recordings. Neighbouring infected and uninfected pairs of pyramidal cells were recorded simultaneously in CA1 with Schaffer collateral stimulation. The AMPAR/NMDAR ratio was calculated as the peak averaged AMPAR EPSC (30–50 consecutive events) at −70 mV divided by the averaged NMDAR EPSC (20–40 consecutive events), measured 50 ms after the onset of the dual component EPSC at +40 mV.

Miniature EPSCs. AMPAR mEPSCs were recorded in the presence of tetrodotoxin (TTX; 0.5 μM) holding the cells at −70 mV (detection threshold, 5 pA). The average mEPSC amplitude and frequency for each cell was calculated by collecting all mEPSCs recorded during the initial 5-min period after whole-cell access when a stable series resistance (10–15 MΩ) was achieved. For the cumulative probability plots of mEPSC amplitude and inter-event interval, the first 200 mEPSCs from each cell were included.

Nucleated outside-out patch recordings. Outside-out patches were pulled from the somata of hippocampal CA1 pyramidal neurons and held at −70 mV. We applied 10 μM of s-AMPA to the patches using a Picospritzer II (Parker Hannifin Corp.) in the presence of 100 μM cyclothiazide, 50 μM picrotoxin, 25 μM AP5 and 0.5 μM TTX.

Controls for slice physiology experiments. For analysis of Syt1 and Syt7 knockdowns using AAV-expressed shRNAs (Fig. 1b), all viruses expressed GFP, and the control slices were obtained from separately infected animals that expressed only GFP without an shRNA (Extended Data Fig. 2). For experiments in constitutive Syt7 knockout mice expressing lentiviral Syt1 knockdown (Extended Data Fig. 3f), controls were separately infected animals that were injected with a lentivirus expressing GFP only. For analysis of Syt1 and Syt7 knockdown using lentivirally expressed shRNAs, conditional Syt1 knockout experiments using lentivirally expressed Cre-recombinase and lentiviral overexpression of the dominant negative Syt1-C2A*B* (Figs 1c, 2a–d, 3a–g, 5f; Extended Data Figs 3d, 6, 7, 9d–h), controls were recorded from uninfected cells located nearby in the same animals and slices as the knockdown cells.

Dissociated hippocampal culture electrophysiology. Cultures of hippocampal neurons were produced from wild-type and Syt1 KO mice, and used for viral infections and recordings at 14–16 DIV as described[16,17,43,44]. Recordings were done blindly.

Organotypic cultures and recordings from cultured hippocampal slices. Organotypic slice cultures were prepared from young Syt1cKO and Syt7 KO mice (P6–7) and placed on semiporous membranes (Millipore) for 5–7 days before recording[25,45]. Voltage-clamp whole-cell recordings were obtained from CA1 pyramidal neurons treated with vehicle control, 10 μM CNQX (for 36 h before recording) or 10 μM retinoic acid (RA) (for 4 h before recording), under visual guidance using transmitted light illumination. Tests and controls were from the same batches of slices on the same experimental day and were analysed as described[25]. CNQX- or RA-treated slices were washed out before evoked responses were recorded.

Chemical LTP (cLTP) assay and immunocytochemistry. We thoroughly washed 18–21 days in vitro (DIV; 9–11 days after infection) hippocampal cultures with extracellular solution (ECS) containing (in mM): 150 NaCl, 2 CaCl₂, 5 KCl, 10 HEPES pH 7.4, 30 glucose, 0.001 TTX, 0.01 strychnine and 0.03 picrotoxin. For cLTP, neurons were incubated with or without 0.3 mM glycine at room temperature for 3 min in ECS, and then for another 20–25 min in ECS without glycine at 37 °C. Neurons were fixed with 4% paraformaldehyde for 15 min on ice, which does not permeabilize the cells. Surface AMPARs were labelled for 1 h at 37 °C with a polyclonal rabbit primary antibody specific to an N-terminal extracellular epitope of GluA1 (Calbiochem) or a mouse monoclonal antibody against an extracellular epitope of GluA2 (MAB397, EMD Millipore); they were washed multiple times with PBS and reacted for 1 h at 37 °C with appropriate secondary antibodies. Confocal stacks were obtained for 6–12 individual fields from multiple coverslips per culture with a 60× 1.4 NA oil-immersion objective mounted on a Nikon A1 laser-scanning confocal microscope. Three independent cultures (control, non-stimulated coverslips and glycine-treated coverslips) were examined for each manipulation.

Synaptic and extrasynaptic GluA1 levels. Wild-type and GluA1-KO cultured neurons were infected with GFP-expressing lentivirus with or without shRNAs at DIV8, and fixed at DIV18–21 in 4% paraformaldehyde and 4% sucrose for 15 min on ice (no permeabilization). Surface GluA1 AMPARs were labelled using a polyclonal rabbit primary antibody specific to an N-terminal extracellular epitope of GluA1 (Calbiochem) and visualized with anti-rabbit Alexa 568-conjugated secondary antibodies. After permeabilizing the cells with 0.1% Triton X-100 for 30 min

at room temperature, a mouse monoclonal anti-PSD-95 antibody (Abcam 2723) was co-applied with an anti-GFP antibody (raised in chicken; Aves Labs) followed by anti-mouse Alexa 647-conjugated and anti-chicken Alexa 488-conjugated secondary antibodies, respectively. Primary and subsequently secondary antibodies were incubated with cells at 37 °C for 1 h spaced with multiple PBS washes. For image acquisition, coverslips were mounted on glass slides in fluoromount-G (Southern Biotech). Confocal stacks were obtained in three-colour channels for 6–12 individual fields from multiple coverslips per culture (three cultures) with a 60× 1.4 NA oil-immersion objective mounted on a Nikon A1 laser-scanning confocal microscope. Imaging and analyses were performed using raw images without knowledge of the experimental manipulation that had been performed. Confocal images were acquired maintaining Nyquist criteria for digital microscopy. A maximum intensity Z projection was obtained from each confocal image stack using custom Nikon software and quantitative image analysis was performed on these images; non-induced control cells from the same culture were used as the baseline for comparisons. Total dendritic surface AMPARs in a field were determined by calculating the total number of pixels enriched in AMPARs above an arbitrary threshold value that was kept constant for all images from that culture preparation and was selected by visual inspection of images from non-induced control cells using ImageJ (http://rsb.info.nih.gov/ij/). This value was divided by the total surface area calculated using a lower threshold value that captured the entire dendritic arbour and that was again kept constant for all images from a culture preparation. To calculate changes in AMPAR surface expression following experimental manipulations, AMPAR surface expression values for each image were normalized to the average value obtained from non-treated control cells for each individual culture preparation. Image thresholds, area measurements and numerical calculations were performed using software developed in Matlab (The MathWorks, Inc.). To identify the synaptic and extrasynaptic fractions of GluA1 staining, Z-projection was obtained from three individual colour images of 50 μm dendritic segments. The total area and synaptic area masks were created by applying threshold values to GFP and PSD95 images, respectively. Then, an extrasynaptic area mask was obtained by subtracting the synaptic area from the total area mask image. These two masks, synaptic and extrasynaptic, were then applied to the GluA1 image to determine the average intensity of GluA1 staining on GluA1-wild-type, Syt1–Syt7 double knockdown and GluA1-KO dendritic segments.

V5-tagged Syt1 and Syt7 immunocytochemistry. Wild-type cultured neurons were transfected at DIV7 using calcium phosphate with constructs expressing either V5-tagged Syt1 or Syt7 and eGFP. Cells were fixed at DIV14–16 in 4% paraformaldehyde and 4% sucrose for 15 min and permeabilized with 0.1% Triton X-100 for 20 min at room temperature. Coverslips were incubated in primary antibodies against V5 (rabbit, V8137, Sigma), MAP2 (mouse, M1406, Sigma) and VGluT1 (guinea pig, ab5905, Millipore); and secondary antibodies anti-mouse AlexaFluor405, anti-rabbit AlexaFluor546 and anti-guinea pig AlexaFluor633. Primary and subsequently secondary antibodies were incubated with cells at 37 °C for 1 h spaced with multiple PBS washes. For image acquisition, coverslips were mounted on glass slides in fluoromount-G. Confocal stacks were obtained in four-colour channels with a 60× 1.4 NA oil-immersion objective.

Endocytosis assay. AMPAR internalization assays were performed essentially as described[46]. After 14–16 DIV, cultured hippocampal neurons were labelled at 37 °C for 20 min with a primary antibody against an extracellular epitope of GluA1 (Calbiochem) or GluA2 (MAB397, Millipore) to allow labelling of surface AMPARs. Cells were washed in PBS, then incubated at 37 °C with neuron growth medium for 20 min to allow basal internalization. Cells were then washed and fixed with 4% PFA and 4% sucrose, blocked in a detergent-free blocking solution for 1 h, and incubated with AlexaFluor546 secondary antibody at room temperature for 1 h to label surface receptors. Neurons were then post-fixed with 100% methanol at −20 °C, blocked for 1 h and incubated with an AlexaFluor633 secondary antibody at room temperature for 1 h to label the internalized AMPAR fraction. Fluorescent images were acquired at room temperature with a Nikon A1 laser-scanning confocal microscope using a 60× 1.4 NA oil-immersion objective. Within the same experiment, the same settings for laser power, PMT gain and offset were used. Digital images were taken using Nikon NIS-Elements imaging software. Data shown represent the average of the mean values from at least three independent experiments. To calculate internalization, the integrated red fluorescence intensity that identifies internalized GluA1 was divided by the total (red and green) intensity and normalized to the averaged wild-type levels.

Glycine treatment of live cells after photobleaching. Hippocampal cultures at DIV7–8 were transfected using calcium phosphate with SEP–GluA1 constructs with or without shRNAs. Live cells on coverslips (DIV18–21) were thoroughly washed and incubated in a live imaging chamber with extracellular solution (ECS) at 37 °C. First, a Z-stack image of an entire transfected neuron was obtained with a 40× 1.3 NA oil-immersion objective mounted on a Nikon A1 laser-scanning confocal microscope. High laser power was used to scan and bleach the whole cell. Immediately after bleaching, another Z-stack image was taken to ensure more than 95% reduction of surface fluorescence intensity. We perfused 500 μM glycine in ECS into the chamber for 3–4 min to induce cLTP, followed by ECS (no glycine) perfusion at 37 °C for 20 min. A series of Z-stack images was obtained after induction at the 5-min interval to capture the fluorescence recovery. Z-projections were obtained from each time point using Nikon's maximum intensity projection method. Multiple time points for images were then stacked together as a time series in ImageJ. Dendritic segments (50 μm) were used to quantify the fluorescence intensity emitted from SEP–GluA1 expressed at the cell surface. A mask of a dendritic segment was created using the first image (pre-bleach) of the time series and then applied to all images to determine the total intensity under the same mask for all three conditions. Each intensity value was normalized with respect to the initial intensity and a graph of the mean ± s.e.m. was made in Microsoft Excel for presentation.

qPCR. To measure mRNA in cultured neurons, RNA was isolated at DIV14 using the RNAqueous kit (Ambion). RT–PCR reactions were set up in duplicate for each condition (150 ng total RNA) using the LightCycler 480 reagent kit (Roche), gene-specific primers (Roche) and a 7900HT Fast RT–PCR instrument (Applied Biosystems) with GAPDH as an internal control.

Immunoblotting. Whole brains were homogenized in PBS with 0.3% Triton X-100 and protease inhibitor cocktail. Lysates were centrifuged at 14,000 rpm at 4 °C for 15 min. We added 20 μl of supernatant to sample buffer and loaded it onto a 10% SDS-containing polyacrylamide gel, which was run at 120 V for 1 h. Proteins on the gel were transferred to a nitrocellulose membrane and incubated in 5% milk blocking solution for 1 h, incubated in a 1:1,000 dilution of primary antibody overnight (Syt7: rabbit S757 Sysy, HA: rat 3F10 Roche, valosin-containing protein (VCP): rabbit K331, actin: mouse a1978 Sigma) and incubated in a 1:10,000 dilution of secondary antibody conjugated to fluorescent probes for 1 h. Proteins were visualized using the Licor Odyssey CLx system.

Data analyses and statistics. Electrophysiology data were analysed with either a custom program written with Igor Pro software (Wavemetrics), MiniAnalysis (Synaptosoft) or Clampfit (Molecular Devices). Statistical significance was assessed by the Mann–Whitney U test for all pairwise comparisons, with the exception of simultaneous dual-cell recordings, for which the Wilcoxon signed rank test was used. Two-way ANOVA was used for the SEP–GluA1 experiment in Fig. 4d. For all other experiments with three or more groups, statistical significance was assessed with the Kruskal–Wallis test; when significant differences were observed, pairwise comparisons were assessed by the Mann–Whitney U test ($*P < 0.05$; $**P < 0.01$; $***P < 0.001$).

Data availability. All relevant data are included with the manuscript as source data or Supplementary Information.

41. Maximov, A. et al. Genetic analysis of synaptotagmin-7 function in synaptic vesicle exocytosis. Proc. Natl Acad. Sci. USA **105,** 3986–3991 (2008).
42. Xu, J., Pang, Z. P., Shin, O. H. & Südhof, T. C. Synaptotagmin-1 functions as a Ca²⁺ sensor for spontaneous release. Nat. Neurosci. **12,** 759–766 (2009).
43. Tang, J. et al. A complexin/synaptotagmin 1 switch controls fast synaptic vesicle exocytosis. Cell **126,** 1175–1187 (2006).
44. Maximov, A., Pang, Z. P., Tervo, D. G. & Südhof, T. C. Monitoring synaptic transmission in primary neuronal cultures using local extracellular stimulation. J. Neurosci. Methods **161,** 75–87 (2007).
45. Gähwiler, B. H., Capogna, M., Debanne, D., McKinney, R. A. & Thompson, S. M. Organotypic slice cultures: a technique has come of age. Trends Neurosci. **20,** 471–477 (1997).
46. Aoto, J., Martinelli, D. C., Malenka, R. C., Tabuchi, K. & Südhof, T. C. Presynaptic neurexin-3 alternative splicing trans-synaptically controls postsynaptic AMPA receptor trafficking. Cell **154,** 75–88 (2013).

Outline and Summary of Experiments

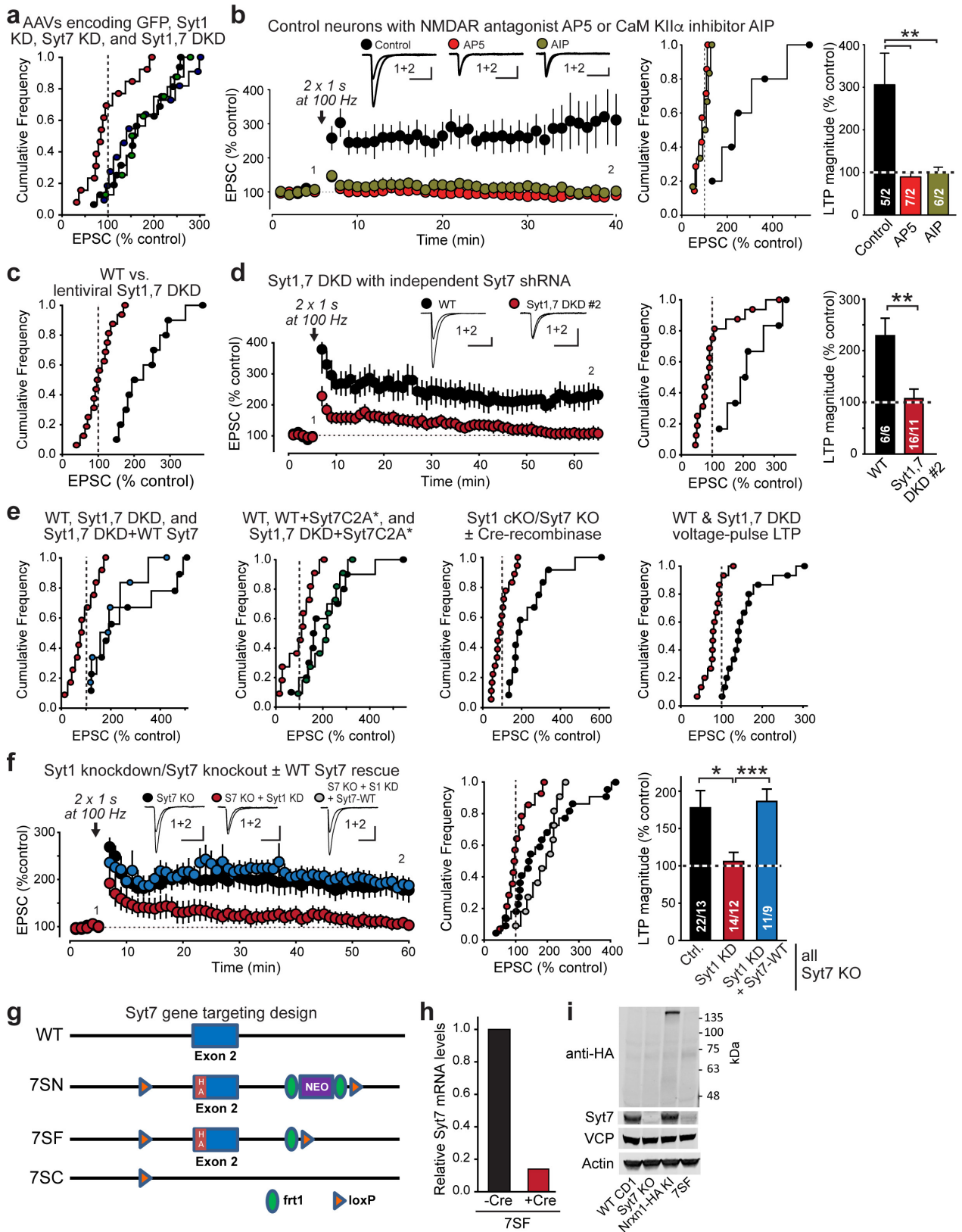| Question	Approach	Results	Controls	Figures
A. Do synapto-tagmins perform an essential function in LTP?	1. Test single and double loss-of-function of Syt1,7 and Syt3,5 using KDs and genetic KOs combined with different LTP protocols 2. Test Syt1,7 double loss-of-function in cLTP measurements	1. Double but not single loss-of-function of Syt1 & Syt7 blocks all types of LTP 2. Double loss-of-function of Syt3,5 has no effect 3. Syt1,7 deficiency blocks cLTP 4. Both Syt1,7 double KDs and double KOs block LTP	1. Single Syt1 or Syt7 and double Syt3,5 deletions have no effect 2. LTP observed in interleaved WT & GFP-expressing cells 3. Block of LTP and cLTP is rescued with WT Syt7 4. LTP and cLTP exhibit correct pharmacologic properties 5. Syt1 & Syt7 can be dendritic	Fig. 1, 2, 4 ED Fig. 3-5
B. Is the essential function of Syt1 & 7 in LTP due to a loss of general synaptic strength?	1. Test effect of postsynaptic Syt1,7 deficiency on synaptic strength 2. Monitor mEPSC frequency as a measure of release 3. Image synaptic AMPARs	1. Postsynaptic double loss-of-function of Syt1 & Syt7 has no effect on synaptic strength 2. Postsynaptic Syt1,7 deficiency does not alter synaptic AMPAR levels	1. Different parameters to measure synaptic strength and neurotrans-mitter release give same results 2. GluA1 KO mice provide a negative control	Fig. 3, 4 ED Fig. 6
C. Do Syt1 & Syt7 mediate LTP via a direct essential function in triggering LTP-induced AMPAR exocytosis?	1. Directly measure effect of Syt1,7 deficiency on AMPAR exocytosis during cLTP 2. Test whether indirect impairments of BDNF secretion account for phenotype	1. Double loss-of-function of Syt1 & Syt7 blocks NMDAR-stimulated AMPAR exocytosis during cLTP 2. BDNF does not rescue LTP in Syt1,7-deficient neurons	1. WT Syt7 rescues cLTP-induced AMPAR exocytosis in Syt1,7-deficient neurons 2. Syt1,7 deficiency does not alter other postsynaptic parameters - a trophic factor would be expected to affect many parameters	Fig. 4 ED Fig. 5
D. Is the essential function of Syt1 & 7 in LTP due to a loss of extra-synaptic AMPARs?	1. Measure synaptic & extrasynaptic steady-state AMPAR levels by electro-physiology (mEPSCs, outside-out patches, evoked EPSCs) + imaging	1. Double Syt1,7 loss-of-function does not alter steady-state synaptic or extrasynaptic AMPAR levels	1. GluA1 KO neurons exhibit massive impairment in extra-synaptic AMPARs as a negative control	Fig. 3, 4 ED Fig. 6, 7
E. Are Syt1 & Syt7 required for other forms of AMPAR trafficking, such as LTD, homeostatic plasticity, or con-stitutive AMPAR surface traffic?	1. Measure other types of synaptic plasticity that are mediated by AMPAR trafficking (homeostatic plasticity, LTD) 2. Measure effect of Syt1,7 deficiency on constitutive AMPAR endocytosis to probe for changes in constitutive AMPAR traffic	1. Double Syt1,7 deficiency has no effect on AMPAR trafficking during other forms of plasticity besides LTP 2. Double Syt1,7 deficiency does not change constitutive AMPAR endocytosis → since surface AMPAR levels are normal, does not change constitutive AMPAR exocytosis	1. Endocytosis was measured for two different AMPARs (GluA1 and GluA2) to ensure validity	Fig. 3 ED Fig. 7, 8
F. Do Syt1 & Syt7 function in LTP as Ca^{2+}-sensors for Ca^{2+}-induced AMPAR exocytosis?	1. Test rescue of LTP block with WT and Ca^{2+}-binding mutant Syt7 2. Develop a tool to selectively suppress Ca^{2+}-triggering but not priming functions of Syt1 & Syt7	1. WT Syt7 but not Ca^{2+}-binding mutant Syt7 rescues LTP after Syt1,7 loss-of-function 2. Ca^{2+}-binding-mutant Syt1 but not Syt7 acts as a selective dominant-negative suppressing Ca^{2+}-triggering but not priming of exocytosis 3. Postsynaptic expression of Ca^{2+}-binding-mutant Syt1 blocks LTP and cLTP in WT neurons	1. WT rescue controls for mutant Syt7 rescues 2. LTP induction mediated by Ca^{2+}-influx via NMDARs or via voltage-gated Ca^{2+}-channels gives identical results 3. Dominant-negative Syt1 mutant does not change surface AMPAR levels 4. Dominant-negative Syt1 mutant does not alter paired-pulse ratio, NMDAR/AMPAR ratio, or mEPSC properties	Fig. 2, 5 ED Fig. 9

Extended Data Figure 1 | Overview of experimental questions, approaches, results and controls. The diagram organizes the goals of the present study into six logically connected questions labelled A–F, and provides an overview of the experimental approaches, results and controls.
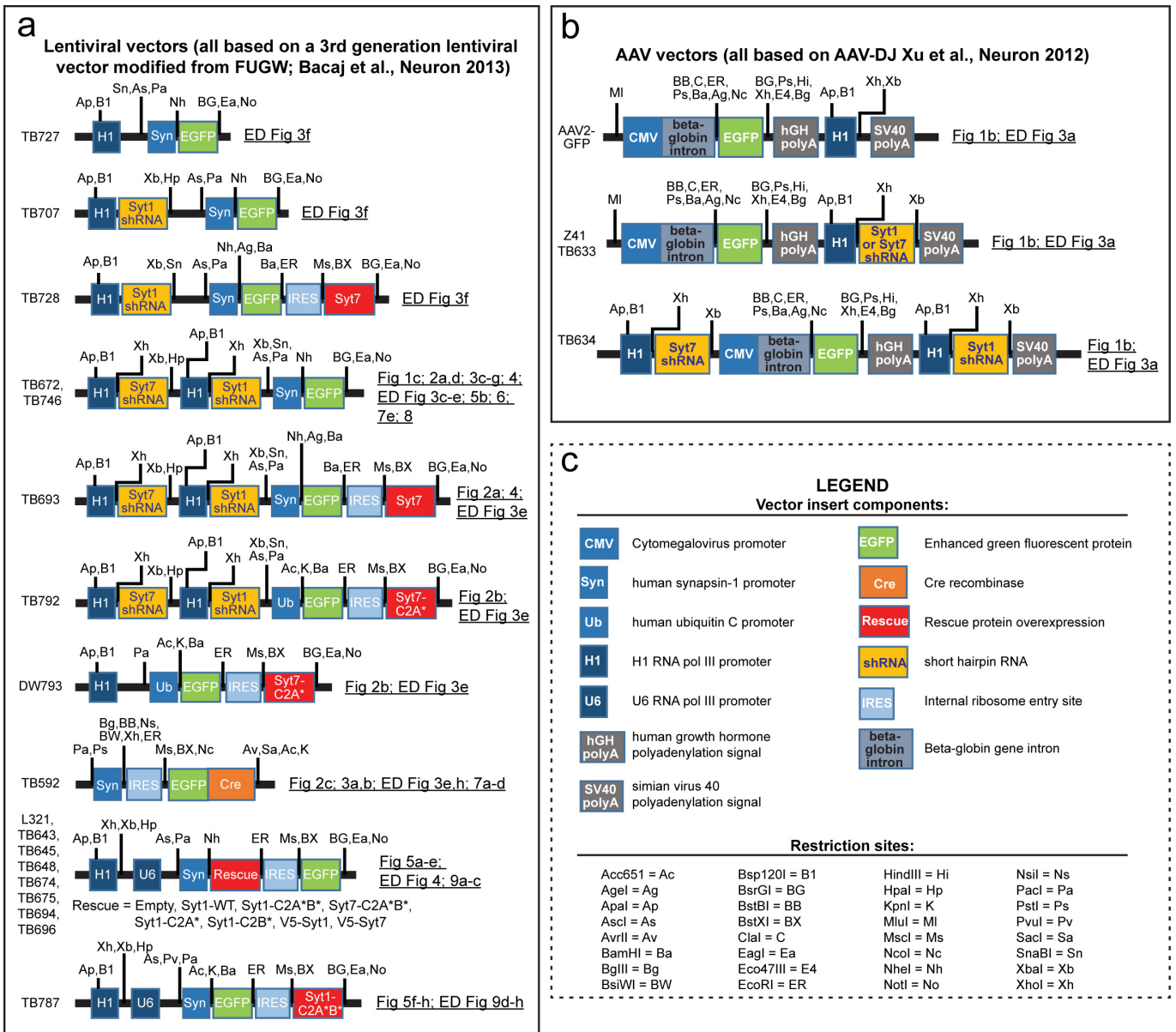
Extended Data Figure 2 | Schematic overview of all viral vectors used in the current study. a, Lentiviral vectors used. Vector names are listed on the left. Backbones are indicated with various insert elements in coloured boxes; promoters and encoded sequences (shRNAs or cDNAs) are colour-coded. Key restriction enzyme sites are shown for mapping and cloning purposes. Figures describing the experiments in which these vectors are used are listed on the right. Drawings are not to scale. Most vectors were described in refs 16, 17 and 19. **b,** Same as **a,** but for AAV vectors. **c,** Legend of vector components and restriction sites found in **a** and **b**.

a AAVs encoding GFP, Syt1 KD, Syt7 KD, and Syt1,7 DKD

b Control neurons with NMDAR antagonist AP5 or CaM KIIα inhibitor AIP

c WT vs. lentiviral Syt1,7 DKD

d Syt1,7 DKD with independent Syt7 shRNA

e WT, Syt1,7 DKD, and Syt1,7 DKD+WT Syt7 | WT, WT+Syt7C2A*, and Syt1,7 DKD+Syt7C2A* | Syt1 cKO/Syt7 KO ± Cre-recombinase | WT & Syt1,7 DKD voltage-pulse LTP

f Syt1 knockdown/Syt7 knockout ± WT Syt7 rescue

g Syt7 gene targeting design

h

i

Extended Data Figure 3 | See next page for caption.

Extended Data Figure 3 | Control experiments for LTP measurements and characterization of a new Syt7 mutant mouse. a, Cumulative frequency plots of LTP magnitude for acute slices from AAV-infected mice expressing control (black), Syt1 knockdown (green), Syt7 knockdown (blue) or Syt1–Syt7 DKD virus (red). Data are from Fig. 1b. **b**, AP5 (50 μM) in the extracellular solution or AIP (20 μM) in the pipette solution impair LTP. Left, representative traces and LTP time course; centre and right, cumulative frequency plots and summary graphs of LTP magnitude. **c**, Cumulative frequency plots of LTP magnitude in acute slices recorded from control (black) and lentivirally infected neurons (red) from mice stereotactically injected with lentiviruses expressing the Syt1–Syt7 DKD. Data are from Fig. 1c. **d**, Lentiviral *in vivo* Syt1–Syt7 DKD with a second, independent shRNA against Syt7 impairs LTP. **e**, Cumulative frequency plots of LTP magnitude for the experiments shown in Fig. 2a–d. In all experiments, black denotes control conditions; in the first and last panels, red denotes Syt1–Syt7 DKD; in the first panel, blue signifies rescue with wild-type Syt7; in the second panel, green and red indicate rescue with the Syt7 C2A-domain mutant with and without Syt1–Syt7 DKD, respectively; in the third panel, red denotes Syt1–Syt7 DKO. **f**, LTP is blocked by postsynaptic knockdown of Syt1 in constitutive Syt7 KO mice, but rescued by wild-type shRNA-resistant Syt7. **g**, Schematic showing the design of the new Syt7 mutant alleles. Using homologous recombination, exon 2 of the mouse Syt7 gene that encodes the transmembrane region was modified to introduce a haemagglutinin (HA) tag between the Syt7 protein N-terminal and the transmembrane region; in addition, a loxP site was introduced into the 5′ intron and a neomycin resistance cassette (NEO) that was flanked by

frt1 sites and was followed by a second loxP site introduced in the 3′ intron. The initial mouse mutant was named 7SN; FLP recombination removed the NEO cassette to produce strain 7SF that should have expressed HA-tagged Syt7 per design but failed to do so (see **i**). 7SF was also designed to serve as a conditional knockout (cKO) in which Cre recombination deletes exon 2 to produce mouse strain 7SC, which represents a true constitutive Syt7 knockout because exon 2 is out-of-frame and encodes the vital transmembrane region. **h**, Lentiviral Cre expression in cultured hippocampal 7SF neurons reduced Syt7 mRNA levels by about 90%, demonstrating that the 7SF neurons express Syt7 mRNA and that the 7SF locus is a conditional knockout. **i**, Immunoblotting of brain homogenates from adult mice with the indicated genotypes using antibodies specific to the HA epitope, Syt7, VCP or actin (the latter two as loading controls) shows that 7SF does not express Syt7 protein. Neither HA antibodies nor Syt7 antibodies detected Syt7 protein in 7SF mice designed to express HA-tagged but otherwise normal Syt7 (see **g**). Immunoblots of proteins from wild-type CD1 mice and from another strain of Syt7 knockout mice were included as positive and negative controls for Syt7, respectively; immunoblots of Nrxn1–HA knockin mice (unpublished) were used as a positive control for the HA epitope immunoblot. Molecular weight markers are indicated on the right. For gel source data, see Supplementary Fig. 1. Data are mean ± s.e.m. (numbers in bars show number of neurons and mice analysed). Statistical significance was assessed in **b** and **f** with the Kruskal–Wallis test followed by pairwise comparisons with the Mann–Whitney *U* test, and in **d** by the Mann–Whitney *U* test (*$P < 0.05$; **$P < 0.01$; ***$P < 0.001$). Calibration bars: 50 pA, 50 ms for **b**, **d** and **f**.
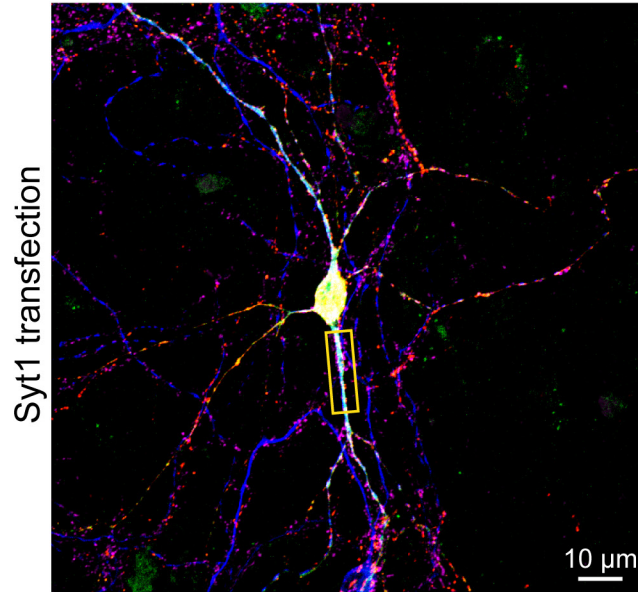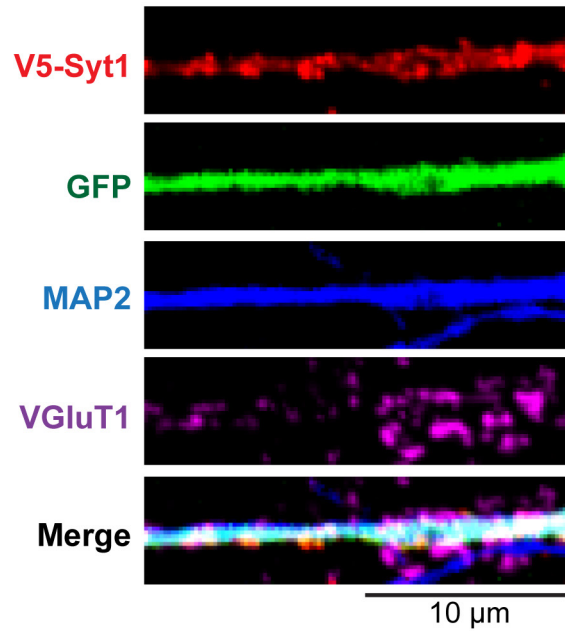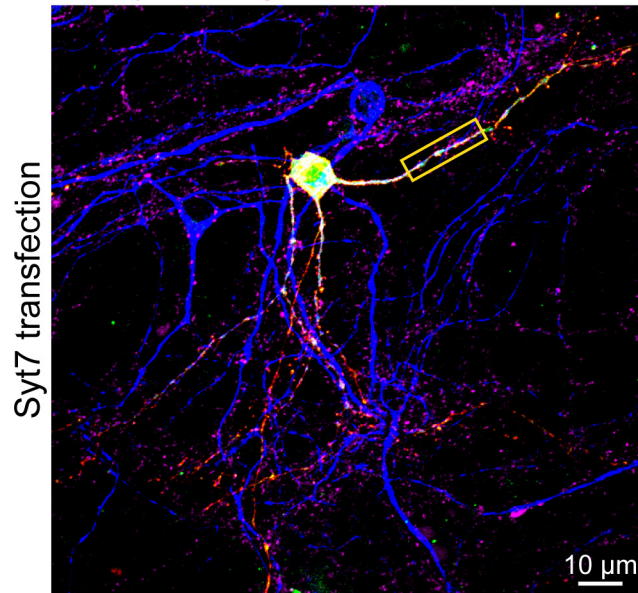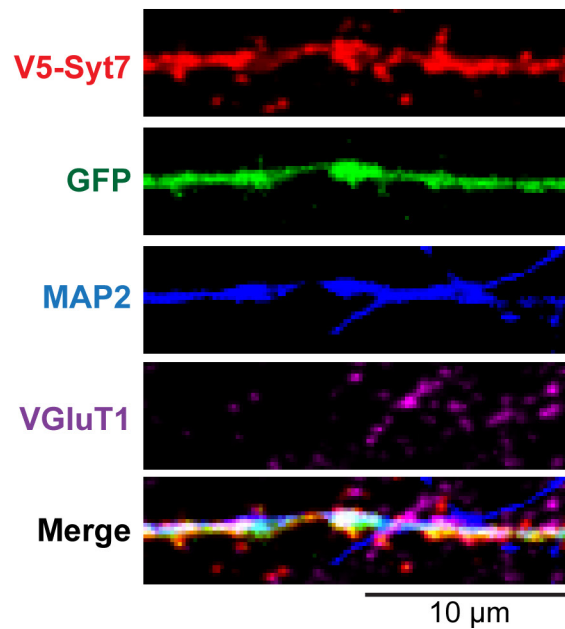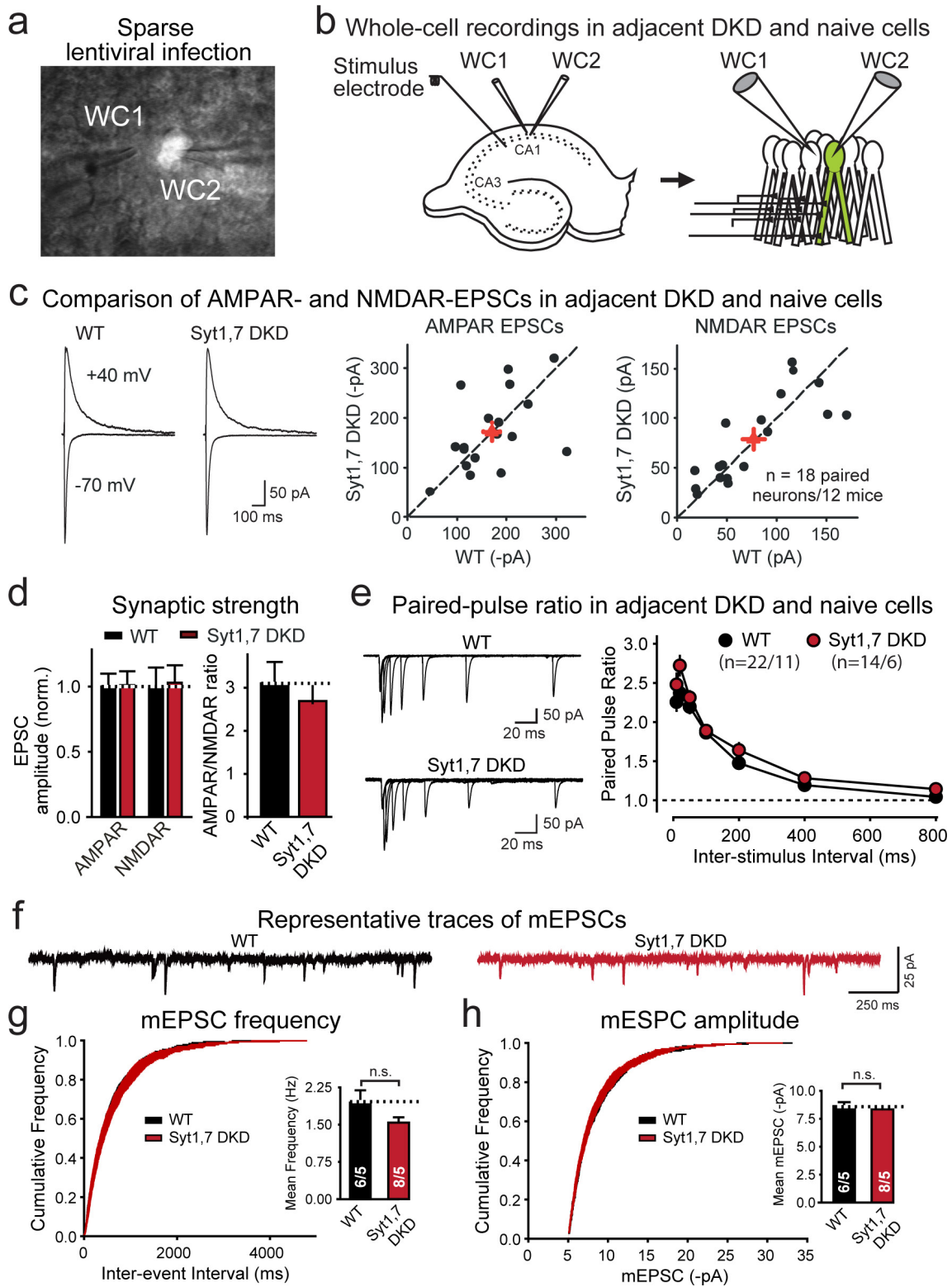
Extended Data Figure 4 | Dendroaxonal localization of Syt1 and Syt7 in cultured hippocampal neurons. a, Representative image of a wild-type cultured hippocampal neuron transfected with a vector co-expressing V5-tagged Syt1 and GFP. Neurons were stained for V5 (red), MAP2 (blue) and VGluT1 (magenta) with GFP in green; the image shows the merged staining for all four markers. **b**, Enlarged images of a segment of the dendrite marked by a yellow box in **a**, illustrating the distribution of individual markers. **c, d**, Same as **a, b**, but for V5-tagged Syt7. Note that overexpressed Syt1 and Syt7 enters the entire dendritic extensions of neurons as well as their axons.
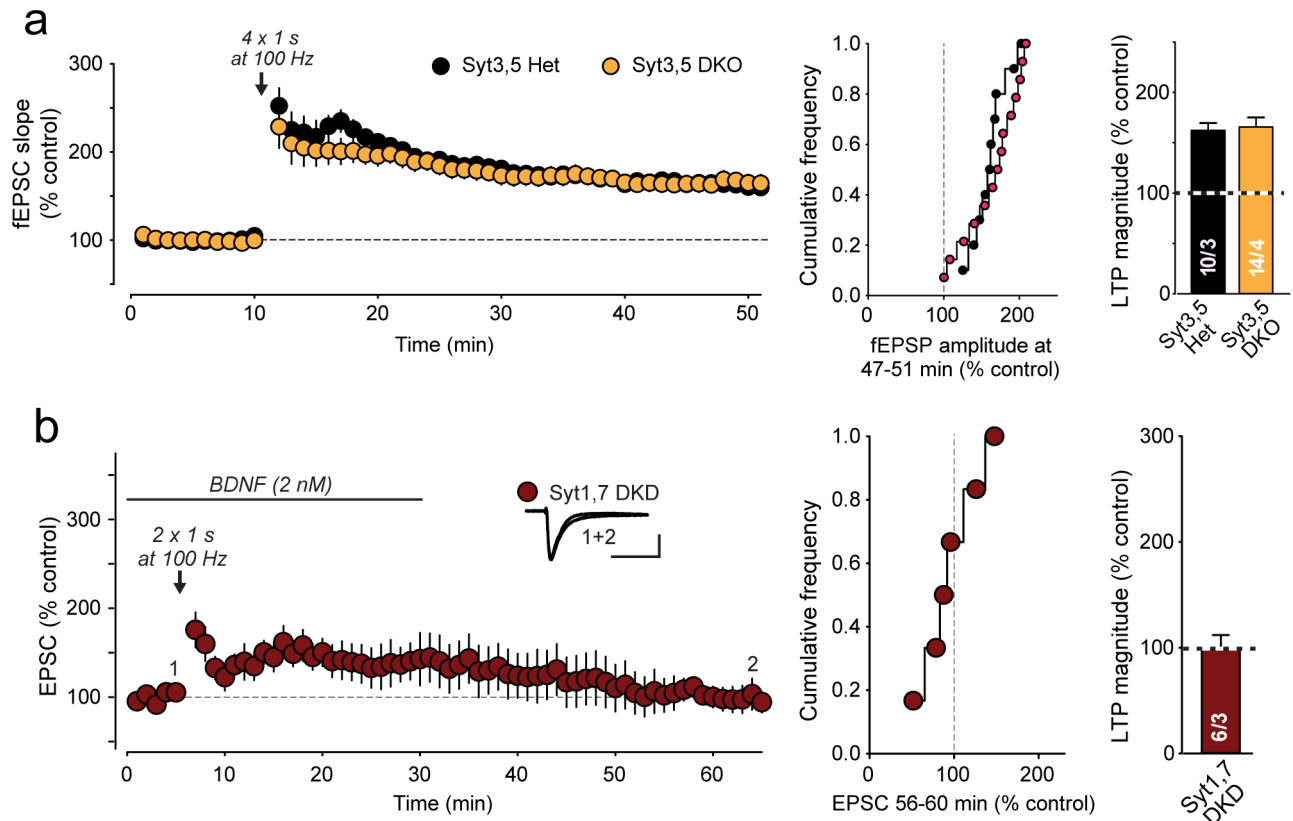
Extended Data Figure 5 | Double deletion of both Syt3 and Syt5 (Syt3–Syt5 DKO) does not alter LTP, and BDNF does not rescue the blocked LTP in Syt1–Syt7 double-deficient neurons. a, Field EPSP (fEPSP) recordings from heterozygous (Syt3,5 Het) and homozygous constitutive Syt3 and Syt5 double knockout mice (Syt3,5 DKO). Left, LTP time course; centre and right, cumulative frequency plots and summary graphs of LTP magnitude. **b**, LTP recordings were performed in Syt1–Syt7 double knockdown cells from acute hippocampal slices as described for Fig. 1. BDNF (2 nM) was applied as indicated. Scale bars below sample EPSCs are 50 pA, 50 ms. All data are mean ± s.e.m.; numbers in bars indicate the number of neurons and mice analysed. Statistical significance in **a** was assessed by the Mann–Whitney U test.

a Sparse lentiviral infection

b Whole-cell recordings in adjacent DKD and naive cells

c Comparison of AMPAR- and NMDAR-EPSCs in adjacent DKD and naive cells

AMPAR EPSCs

NMDAR EPSCs

n = 18 paired neurons/12 mice

d Synaptic strength

e Paired-pulse ratio in adjacent DKD and naive cells

f Representative traces of mEPSCs

g mEPSC frequency

h mESPC amplitude

Extended Data Figure 6 | See next page for caption.

Extended Data Figure 6 | Postsynaptic Syt1–Syt7 ablation does not impair basal synaptic transmission or alter short-term plasticity, and does not affect the amplitude or frequency of spontaneous mEPSCs in CA1-region pyramidal neurons. a, b, Fluorescence image of a slice with patched adjacent non-fluorescent uninfected and fluorescent infected neurons (**a**), and schematic of simultaneous whole-cell recordings from uninfected and infected Syt1–Syt7 DKD pyramidal neurons (**b**). **c,** Syt1–Syt7 DKD does not decrease NMDAR- and AMPAR-mediated synaptic transmission (left, representative AMPAR- and NMDAR-EPSCs; right, scatter plots of dual recordings; red crosses show mean ± s.e.m.). **d,** Normal AMPAR/NMDAR ratios in Syt1–Syt7 DKD neurons (left, summary graphs of AMPAR- and NMDAR-mediated EPSCs; right, summary graphs of AMPAR/NMDAR ratios). **e,** Syt1–Syt7 DKD does

not cause major changes in the paired-pulse ratio (left, representative traces; right, summary plot of the paired-pulse ratio versus inter-stimulus interval). **f–h,** Lentiviral *in vivo* Syt1–Syt7 DKD has no significant effect on the frequency or amplitude of spontaneous mEPSCs. Representative mEPSC traces are shown in **f**; cumulative plots of the inter-event interval and summary graphs of the mEPSC frequency are displayed in **g**, and cumulative plots and summary graphs of the mEPSC amplitude in **h**. Data are mean ± s.e.m. (numbers in bars or graphs show number of neurons and mice analysed; numbers for **c** also apply to **d**). Statistical significance in **d** was assessed by Wilcoxon signed rank test for normalized amplitude and the Mann–Whitney *U* test for AMPAR/NMDAR ratios, and in **e, g** and **h** by the Mann–Whitney *U* test.
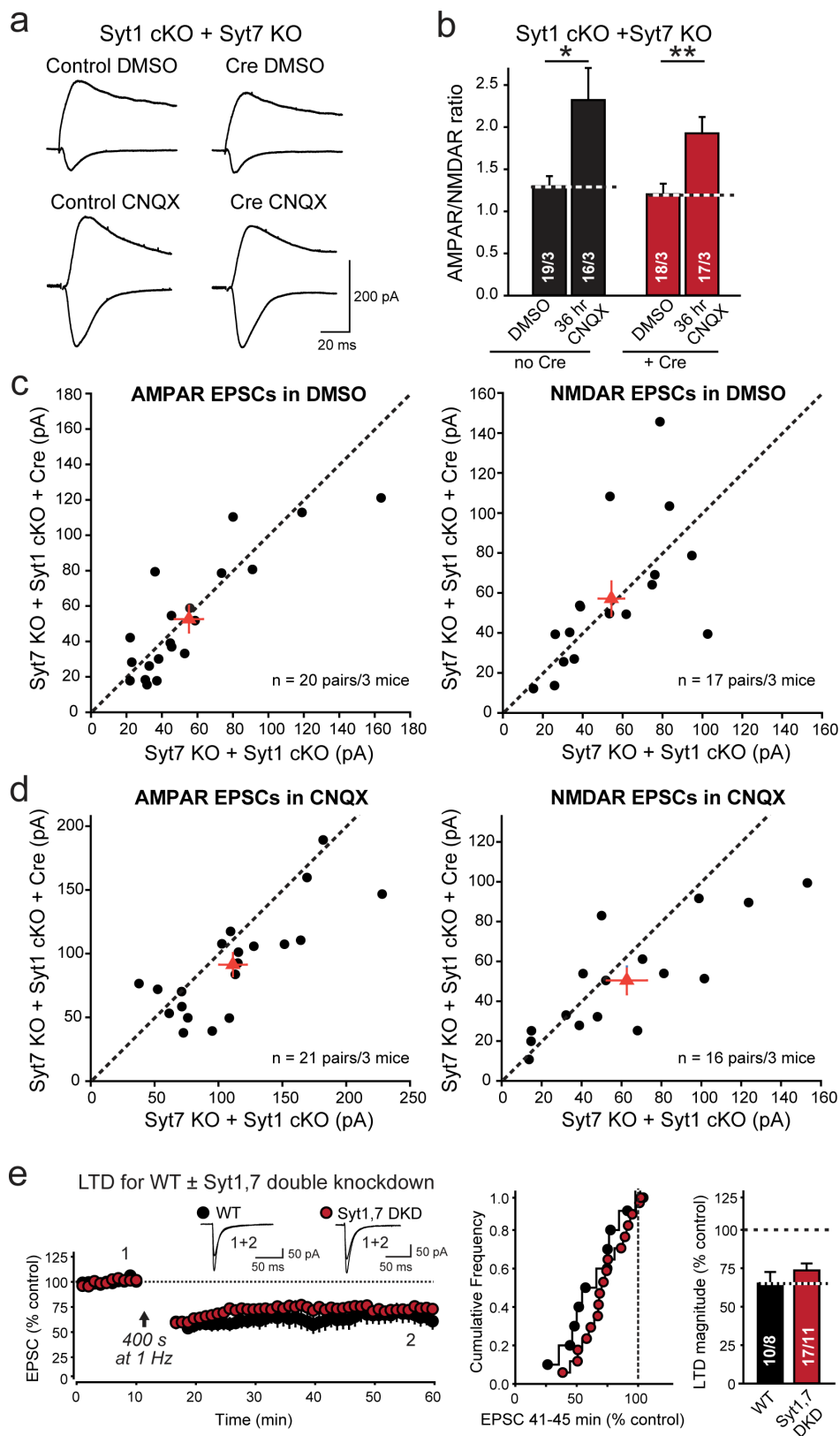
Extended Data Figure 7 | Retinoic acid-dependent homeostatic plasticity and LTD are normal in Syt1–Syt7 double-deficient neurons.
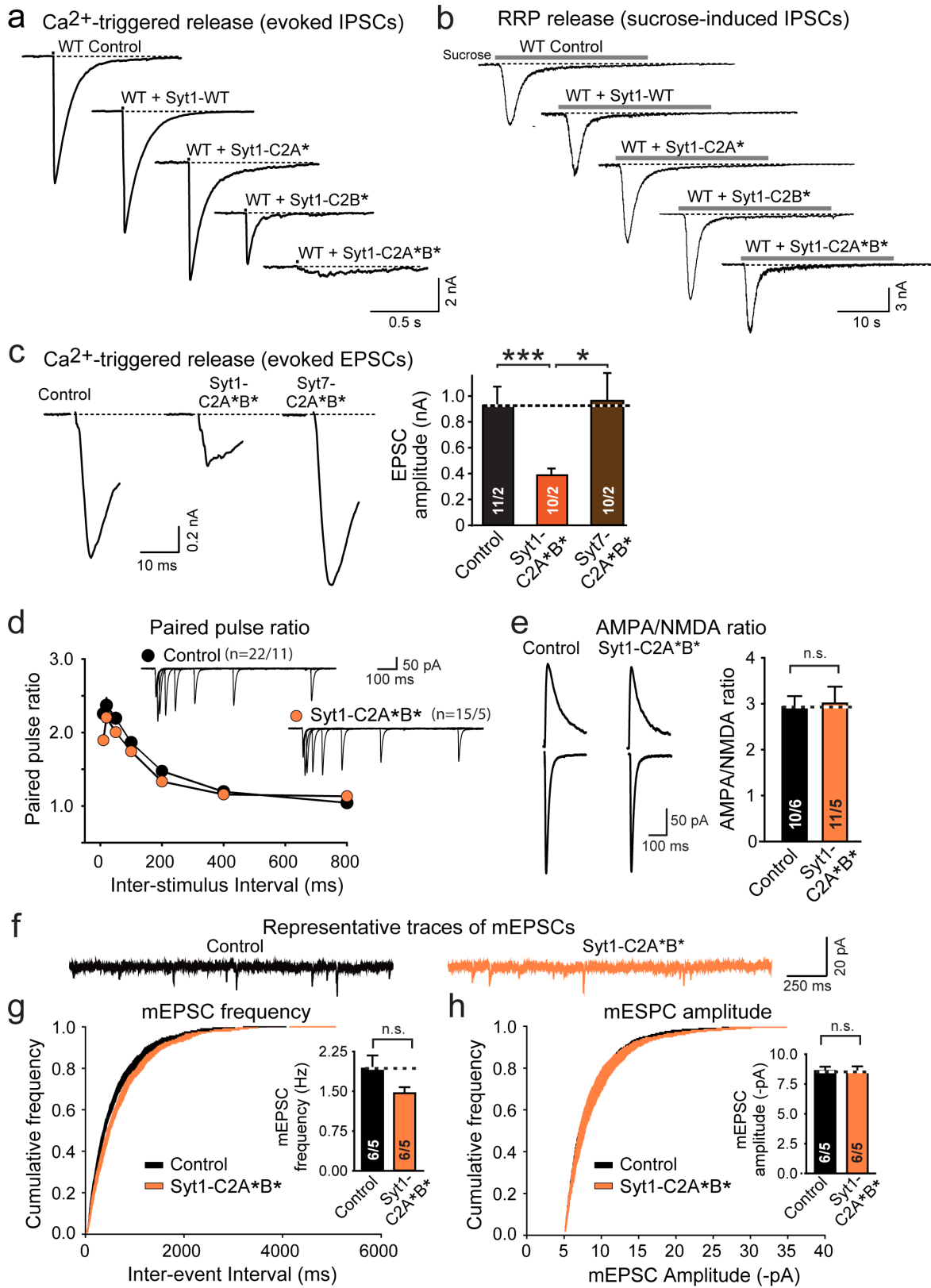**a**, Representative traces of evoked AMPAR- and NMDAR-mediated EPSCs in dual recordings of infected Cre and uninfected adjacent neurons in the same cultured hippocampal slice that had been incubated for 36 h in DMSO and CNQX. **b**, Summary graph of AMPAR/NMDAR ESPC ratios calculated from the EPSCs monitored in **a**. **c**, **d**, Scatter plots of individual dual recordings of AMPAR and NMDAR EPSCs in Syt1–Syt7

DKD and control neurons in slices that had been incubated in DMSO or CNQX. **e**, Syt1–Syt7 DKD does not alter NMDAR-dependent LTD (left, representative traces and time course of induced LTD; centre and right, cumulative frequency plots and summary graphs of the LTD magnitude). All data are mean ± s.e.m.; numbers in bars indicate the number of neurons and mice analysed. Statistical significance was assessed by the Mann–Whitney U test comparing the test conditions to the controls (*$P < 0.05$; **$P < 0.01$).
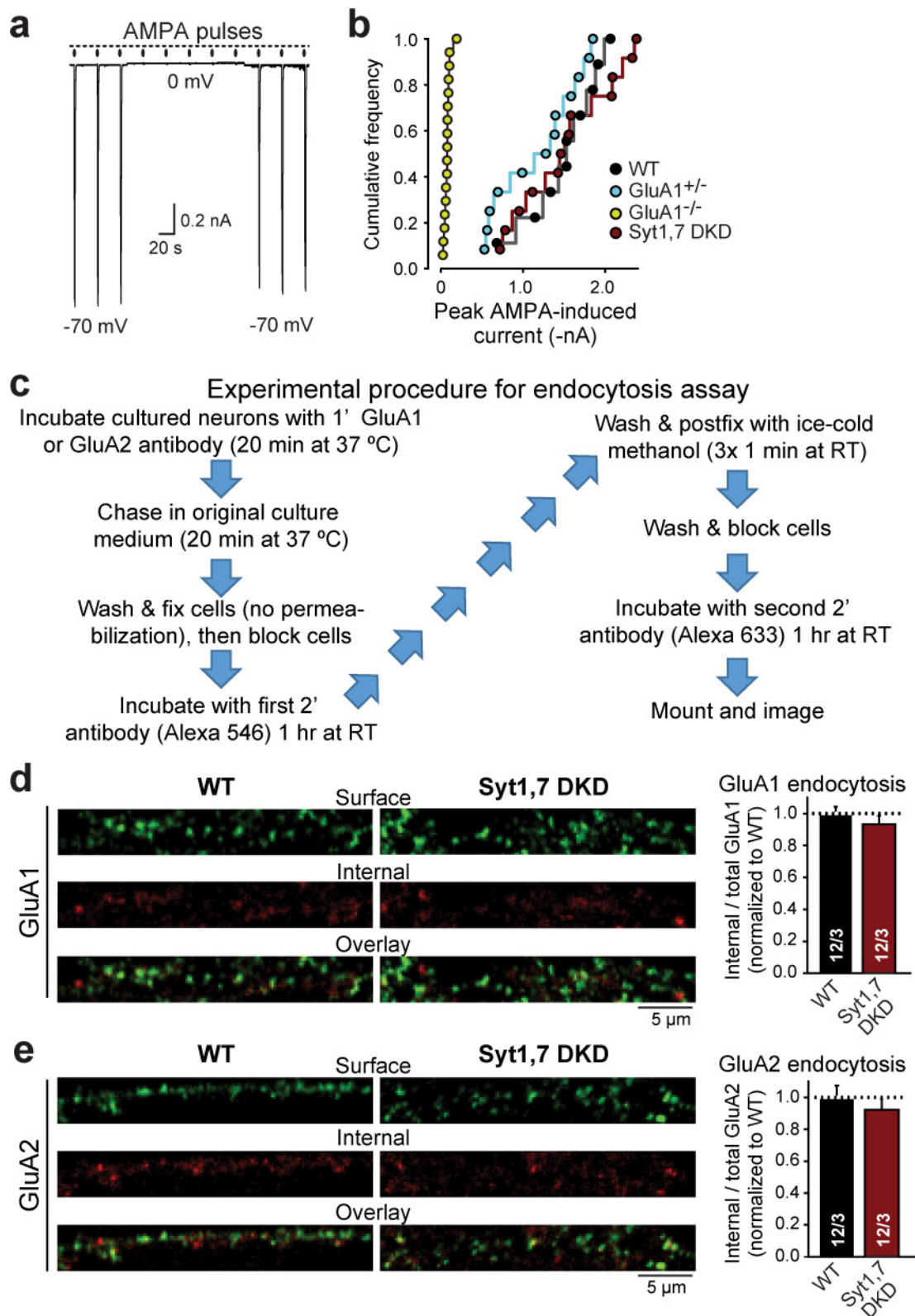
Extended Data Figure 8 | Measurements of GluA1 and GluA2 endocytosis in control and Syt1–Syt7 double-deficient cultured hippocampal neurons. a, Representative traces showing that AMPA-puff-induced net currents in nucleated outside-out patch are blocked at a 0-mV holding potential. **b,** Cumulative frequency plot of the mean peak current amplitude induced by AMPA puffs in nucleated outside-out patches. Note that the only condition that decreases such currents in all independent experiments is the homozygous GluA1 KO (*GluA1*$^{-/-}$). **c,** Experimental procedure flowchart for the endocytosis assay.

See methods for detailed protocol. **d,** Representative images of GluA1 endocytosis in control and Syt1–Syt7 DKD neurons (left), and quantification of GluA1 endocytosis (right). Endocytosis was measured as the ratio of the internal GluA1 fraction (red) to the total GluA1 fraction (internal (red) and surface (green)), and was normalized to the wild type. **e,** Same as **d,** but for GluA2. All data are mean ± s.e.m.; numbers in bars indicate the number of neurons and mice analysed. Statistical significance was assessed by the Mann–Whitney *U* test comparing test conditions to the control.

a Ca²⁺-triggered release (evoked IPSCs)

b RRP release (sucrose-induced IPSCs)

c Ca²⁺-triggered release (evoked EPSCs)

d Paired pulse ratio

e AMPA/NMDA ratio

f Representative traces of mEPSCs

g mEPSC frequency

h mESPC amplitude

Extended Data Figure 9 | See next page for cation.

Extended Data Figure 9 | Presynaptic and postsynaptic expression of dominant-negative Syt1-C2A*B*. a, b, Action potential-evoked (**a**) and sucrose-induced IPSCs (**b**) from cultured hippocampal wild-type neurons infected with control lentiviruses or lentiviruses encoding the indicated Syt1 or Syt7 constructs. In culture, lentiviruses infect all neurons uniformly; thus, recordings reflect conditions in which lentiviruses had infected both pre- and postsynaptic cells. **c**, Evoked EPSCs recorded in cultured wild-type neurons that were infected either with a control lentivirus or with lentiviruses encoding the equivalent mutants of Syt1 (Syt1-C2A*B*) or Syt7 (Syt7-C2A*B*). Note that only the Syt1 but not the Syt7 mutant is dominant negative (left, representative traces; right, summary graph of the EPSC amplitude). **d–h**, *In vivo* expression of dominant-negative Syt1-C2A*B* in postsynaptic neurons alone does not affect basal transmission. Postsynaptic overexpression of dominant-negative mutant Syt1-C2A*B* in a subset of CA1-region pyramidal neurons by stereotactic injection of lentiviruses does not cause a major change in paired-pulse ratios of AMPAR EPSCs at different inter-stimulus intervals (**d**), AMPAR/NMDAR ratio (**e**), or frequency or amplitude of mEPSCs (**f**, sample traces; **g**, cumulative probability plot of the mEPSC inter-event interval with the summary graph of the mean frequency; **h**, cumulative probability plot of the mEPSC amplitude with the summary graph of the mean amplitude). All data are mean $\pm$ s.e.m.; numbers in bars indicate the number of neurons and mice analysed. Statistical significance was assessed in **c** by the Kruskal–Wallis test followed by pairwise comparisons by the Mann–Whitney *U* test (*P < 0.05; ***P < 0.001), and in **d–h** by the Mann–Whitney *U* test only.
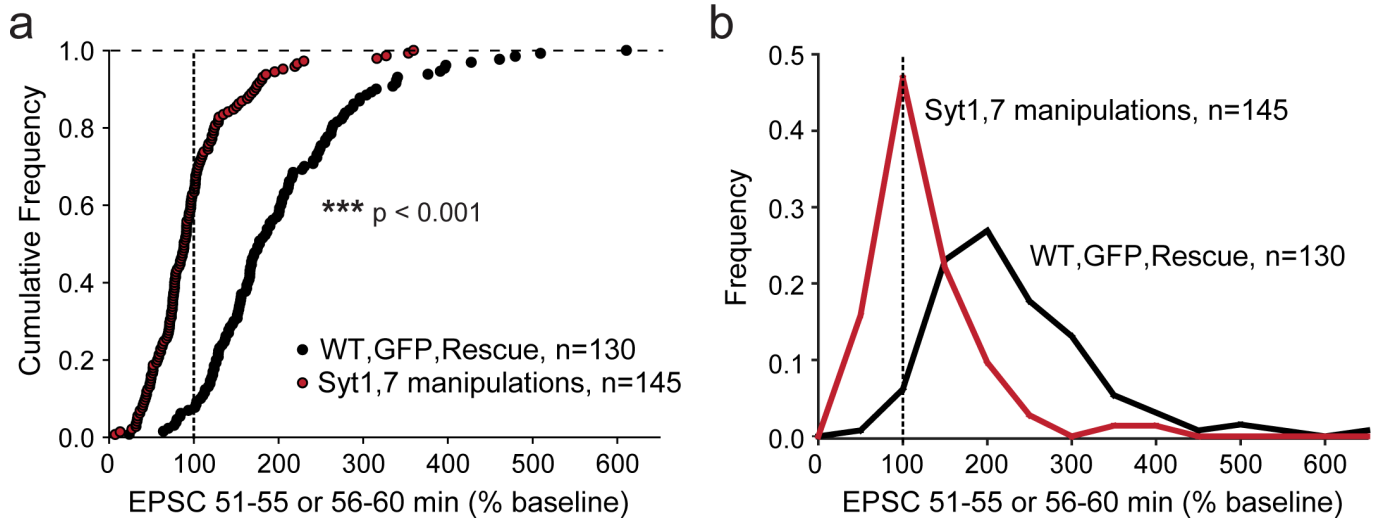
Extended Data Figure 10 | Summary graphs of the combined effects of all Syt1–Syt7 loss-of-function manipulations on postsynaptic LTP. a, Cumulative data for all LTP and voltage-pulse LTP experiments. Statistical significance was assessed by the Mann–Whitney *U* test

(***$P < 0.001$) comparing the test conditions to the control. The dotted line represents the 100% mark corresponding to a lack of change in the synaptic strength as a function of LTP induction. **b**, Normalized frequency of the data in **a** grouped in bins of 50%.